DOC
United States
Department of
Commerce

National Oceanic and
Atmospheric Administration
Seattle WA 98115

EPA
United States
Environmental Protection
Agency

Office of Environmental
Engineering and Technology
Washington DC 20460

EPA-600/7-80-168
October 1980

Research and Development

A Comparison of the Mesa-Puget Sound Oil Spill Model with Wind and Current Observations from August 1978

Interagency Energy/Environment R&D Program Report

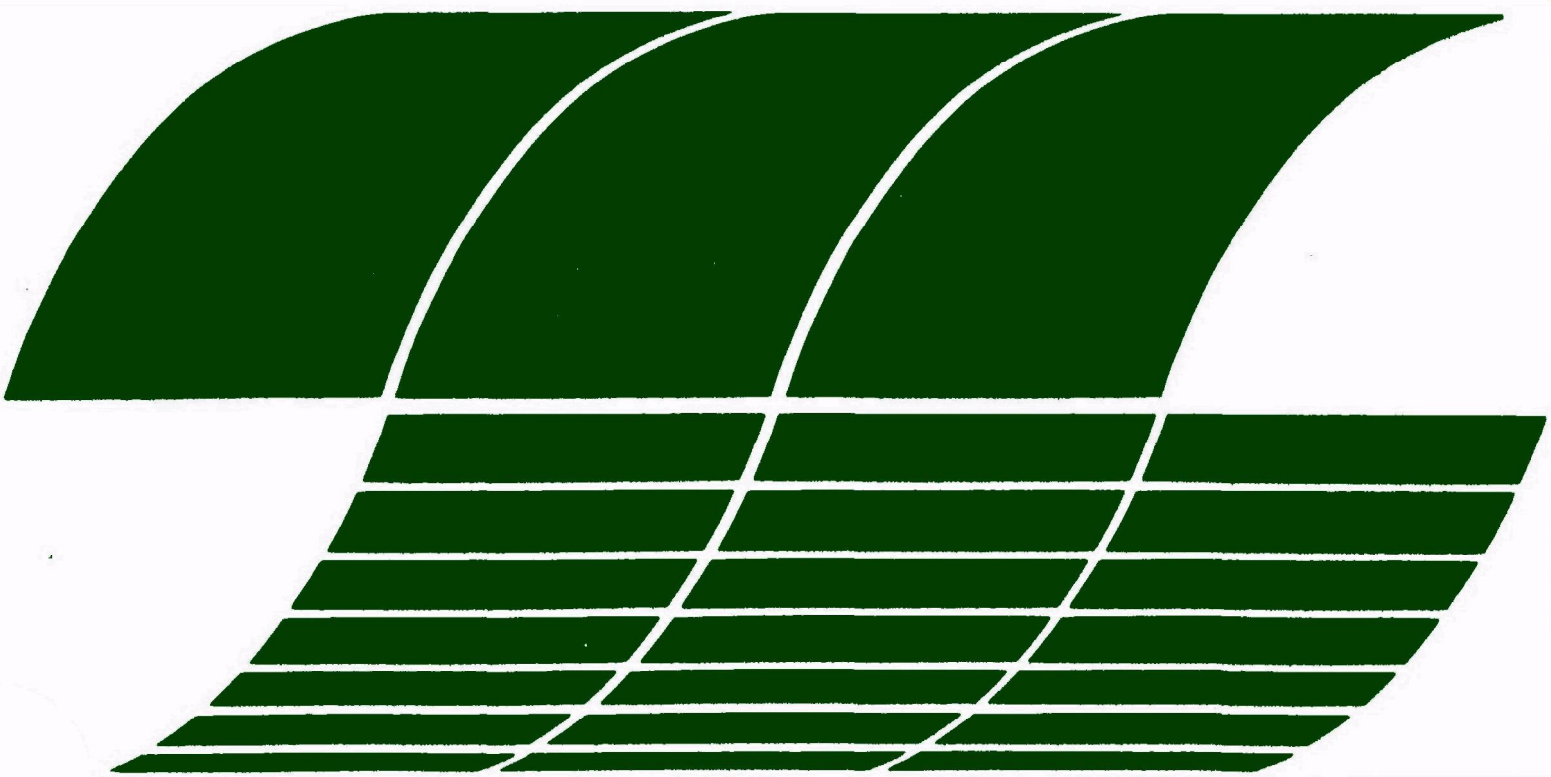

RESEARCH REPORTING SERIES

Research reports of the Office of Research and Development, U.S. Environmental Protection Agency, have been grouped into nine series. These nine broad categories were established to facilitate further development and application of environmental technology. Elimination of traditional grouping was consciously planned to foster technology transfer and a maximum interface in related fields. The nine series are:

1. Environmental Health Effects Research
2. Environmental Protection Technology
3. Ecological Research
4. Environmental Monitoring
5. Socioeconomic Environmental Studies
6. Scientific and Technical Assessment Reports (STAR)
7. Interagency Energy-Environment Research and Development
8. "Special" Reports
9. Miscellaneous Reports

This report has been assigned to the INTERAGENCY ENERGY-ENVIRONMENT RESEARCH AND DEVELOPMENT series. Reports in this series result from the effort funded under the 17-agency Federal Energy/Environment Research and Development Program. These studies relate to EPA's mission to protect the public health and welfare from adverse effects of pollutants associated with energy systems. The goal of the Program is to assure the rapid development of domestic energy supplies in an environmentally-compatible manner by providing the necessary environmental data and control technology. Investigations include analyses of the transport of energy-related pollutants and their health and ecological effects; assessments of, and development of, control technologies for energy systems; and integrated assessments of a wide range of energy-related environmental issues.

This document is available to the public through the National Technical Information Service, Springfield, Virginia 22161.

A COMPARISON OF THE MESA-PUGET SOUND OIL SPILL MODEL WITH WIND AND CURRENT OBSERVATIONS FROM AUGUST 1978

by

Robert J. Stewart
Carol H. Pease

Pacific Marine Environmental Laboratory
Environmental Research Laboratories
National Oceanic and Atmospheric Administration
3711 15th Ave. N.E.
Seattle, Washington 98105

Prepared for the MESA (Marine Ecosystems Analysis) Puget Sound Project, Seattle, Washington in partial fulfillment of

EPA Interagency Agreement No. D6-E693-EN
Program Element No. EHE625-A

This study was conducted
as part of the Federal
Interagency Energy/Environment
Research and Development Program

Prepared for

OFFICE OF ENERGY, MINERALS, AND INDUSTRY
OFFICE OF RESEARCH AND DEVELOPMENT
U.S. ENVIRONMENTAL PROTECTION AGENCY
WASHINGTON, D.C. 20460

AUGUST 1980

Completion Report Submitted to
PUGET SOUND ENERGY-RELATED RESEARCH PROJECT
OFFICE OF MARINE POLLUTION ASSESSMENT
NATIONAL OCEANIC AND ATMOSPHERIC ADMINISTRATION

by

Pacific Marine Environmental Laboratory
Environmental Research Laboratories
National Oceanic and Atmospheric Administration
3711 15th Ave. N.E.
Seattle, Washington 98105

This work is the result of research sponsored by the Environmental Protection Agency and administered by the National Oceanic and Atmospheric Administration.

The National Oceanic and Atmospheric Administration does not approve, recommend, or endorse any proprietary product or proprietary material mentioned in this publication. No reference shall be made to the National Oceanic and Atmospheric Administration or to this publication in any advertising or sales promotion which would indicate or imply that the National Oceanic and Atmospheric Administration approves, recommends, or endorses any proprietary product or proprietary material mentioned herein, or which has as its purpose to be used or purchased because of this publication.

CONTENTS

Figures iv
Tables v
Abstract vi
Acknowledgements vii

1. Introduction 1

2. Conclusions 2

3. Recommendations 4

4. Tidal Current Simulation 6
   Functional Validation of Model 6
   Accuracy of the Model's Interpolation Scheme 7

5. Significance of the Current Model Errors 13
   CASE 1: No Knowledge of Tides 14
   CASE 2: No Knowledge of Nontidal Current 19
   CASE 3: Existing Model with Assumed Steady Current 22

6. Wind Field Simulation 23
   Significance of the Wind Model Errors 26

7. Drifter Response Studies 28

8. References 32

APPENDICES

A. Calculation of Tidal Phase and Amplitude from Model Coeficients 34
B. Moments for Randomly Oriented Constituent Displacements 36

FIGURES

Number		Page
1.	Location of Straits 11, 12, and 13, and the weighting factors applied to Parker's stations	38
2.	Dispersion envelopes assuming no knowledge of tidal currents (Case 1)	39
3.	Tide model contribution to reducing position error relative to Case 1	40
4.	Dispersion envelopes associated with ignorance of high-frequency nontidal current oscillations (Case 2)	41
5.	Observed net currents at various locations in the Strait of Juan de Fuca and the Central Basin	42
6.	Dispersion caused by randomly oriented net current of .66 km/hr (Case 2)	43
7.	A comparison of Case 1 and Case 2 errors	44
8.	Difference-current dispersion ellipses at 1, 3, and 10 hours	45
9.	Wind Pattern No. 3	46
10.	Wind Pattern No. 4	47
11.	Wind Pattern No. 5	48
12.	Wind station locations	49
13.	Principal components of surface wind observations	50
14.	Scatter plot of principal component weights	51
15.	Scatter plot of wind observations, sorted by pattern type at four central basin stations	52
16.	a. Average residual currents on August 25, 1978 (residual = drifter-model)	53
	b. Average residual currents on August 26, 1978 (residual = drifter-model)	54

TABLES

Number		Page
1.	A comparison of a tidal analysis of model output with an analytical prediction based on model coefficients	8
2.	A comparison of simulated tidal currents with actual observations at Straits 11, 12, and 13	9
3.	A comparison of linear interpolation errors with observed model errors	12
4.	Tidal constituent analysis of model errors	18
5.	Parameters for the discrete frequency simulation of the nontidal oscillatory currents	20

ABSTRACT

This report compares the winds and currents observed in August 1978 in the Strait of Juan de Fuca with simulated wind and current fields taken from the MESA-Puget Sound oil spill model. This model is described in a companion report, Pease (in press). A method is developed for relating these errors in velocity to uncertainties in predicted position. The tidal current subprogram of the oil spill model is shown to reduce the uncertainty in trajectory position by an amount that is somewhere in the range of 50% to 90% of the total uncertainty that can be caused by ignorance of the tides. It is also shown that the uncertainty in trajectory position is strongly affected by our inability to predict the baroclinic motions in the region. Over times less than 10 hours, the dispersion is mainly tidal, and the tidal current subprogram contributes significantly to the prediction of position. After 10 hours, however, the bulk of the dispersion is due to the low-frequency (periods longer than a week) baroclinic motions. These baroclinic motions are poorly understood, and a program of basic research directed at illuminating their causes and statistical properties is called for, if predictions are to be made over periods longer than 10 hours. The regional wind model developed by Overland, Hitchman, and Han (1979) and used as a subprogram in the model is compared with wind observations from a short period of time. We conclude that the selection of a master station for use in scaling the pattern strength cannot be done in an arbitrary fashion. We also find that the repertoire of patterns presently available in the program library is not sufficiently comprehensive to allow reliable modeling of the surface winds.

ACKNOWLEDGEMENTS

The authors are most grateful to Ms. Rita Chin who has labored diligently over the computer analysis of the many diverse data sources incorporated in our study. Ms. Chin also prepared the draft figures and was of general assistance throughout the course of this project. Our thanks also to Ms. Sue Larsen who prepared this manuscript and Ms. Virginia May who prepared the figures.

We are indebted to Dr. James E. Overland, Mr. James R. Holbrook, Mr. Carl A. Pearson, and Dr. Harold O. Mofjeld, all of PMEL, for their contributions of data, computer programs, and meteorological and oceanographic expertise. Mr. Pearson was most helpful in providing his time and computer programs for the tidal and spectral analysis of the various current velocity time series. Mr. Holbrook provided us with the current meter observations from Straits 11, 12, 13 and further gave us his own analyses of these data which we have used in several places. Mr. Holbrook's interpretations of the data and his review of portions of our manuscript were of great value to us. Dr. Mofjeld has provided advice on a number of items, and his review of our manuscript resulted in several changes which improved the report.

SECTION 1

INTRODUCTION

In early 1978, an oil spill trajectory model was completed at the Pacific Marine Environmental Laboratory (PMEL) for the MESA-Puget Sound project office. This model is described in Pease (in press). The model was developed under the direction of Dr. Jerry A. Galt, then of PMEL. The model was developed for two main purposes. In the event of an actual oil spill, it is to be used to assist in the cleanup operations. In this mode the model would predict locations and times of arrival of portions of the spill. This information could then be used to improve the deployment of cleanup equipment. The model is also intended for use in a simulation capacity. The site selection of new petroleum transshipment facilities, refineries, or storage facilities involves the consideration of a number of factors, including probable environmental impacts. It was anticipated that the model predictions would be of value in comparing alternative facility locations.

Given the oceanographic complexity of the region the creators of the model did not aspire to comprehensiveness. However, they did wish to exploit the substantial literature on tidal currents that was available as a result of a long-term program of current meter studies by the National Ocean Survey (NOS) (Parker, 1977; NOS, 1973a; NOS, 1973b; NOS, 1979; and by Parker within Cannon (ed.), 1978). It was felt that a fine-scale model based on interpolation and extrapolation of the NOS tidal harmonic analyses would be a good start toward the development of a capability to predict and simulate current behavior.

The details of the surface winds were also little understood. But the concurrent development of a regional wind model (Overland, Hitchman, and Han 1979), offered hope of simulating this complicated variable at a level of detail commensurate with the intended resolution of the model.

Thus, the model development was undertaken not as the final step in a definitive summary of regional oceanography and meteorology, but rather as a first step at attempting to integrate these phenomena. The philosophy underlying this effort rested mainly on the engineer's empiricism, "let's do what we can," rather than a more scientific appraisal of the possibilities.

In late August of 1978, a cooperative oceanographic experiment was undertaken in the region just north of Dungeness Spit (see Frisch, Holbrook, and Ages, 1980). The experiment consisted of drifter motion studies, CODAR and current meter measurements, CTD casts, and surface wind measurements. The results of this experiment provided a good opportunity to examine the wind and current simulation portions of the oil spill trajectory model, and so this study was begun.

SECTION 2

CONCLUSIONS

Two questions were posed: is the current simulation accurate enough to be useful, and is the wind properly modelled using the pattern method? Both questions can be addressed from two viewpoints. First, is the technique properly implemented in the existing model, and secondly, is the modelling concept valid? The implementation question is simply an independent check that the model operates on its input data and coefficient arrays in a fashion consistent with the equations that comprise the model. The modelling concept question is deeper and more philosophical. The model was created to exploit the availability of both the tidal current data and the regional wind model. Little thought has been given to the adequacy of these representations. We have attempted to quantify the contributions these submodels make to reducing the uncertainty of a trajectory prediction, and we have made recommendations for both the interpretation of existing model results and subsequent modelling efforts.

A major difficulty we encountered in addressing the modelling concept question was the determination of what constituted an acceptable error. This problem included both the definition of the error in terms of the various parameters that enter the problem and the interpretation of the error parameter. We have attempted a novel analysis of this problem for the current simulation subprograms. We have shown that a useful measure of trajectory dispersion is the variance of the time-integrated difference between the actual and simulated velocities. This integrated difference-velocity is a displacement, and the variance of this displacement is a measure of the area surrounding a predicted position in which a drifting object is likely to be found.

In order to put into perspective the tidal current subprogram's contribution to trajectory prediction calculations, we have analyzed the displacement errors for three illustrative cases. Case 1 considers trajectory predictions made with perfect knowledge of nontidal currents but completely ignoring tidal currents. The area of the resultant dispersion is shown in Figure 2. Figure 3 depicts the reduction in the tidal dispersion that should be achieved through use of the model, based on our estimates of the model's errors. Figures 4, 5, and 6 treat the converse case, case 2, in which trajectory predictions are made with perfect knowledge of tidal currents and no knowledge of the nontidal currents. Figure 6 graphically illustrates the importance of the nontidal, slowly varying currents caused by density variations within the region.

These slowly varying currents appear as net flows in the 15- and 29-day current meter observations that are used to estimate the amplitude and phase

of the tidal-current constituents. These baroclinic motions are not well understood, and modelling them appears to be a topic of state-of-the-art research. There seems to be no way of dealing with these currents except to hypothesize a particular steady-current field. Figure 8 depicts the trajectory dispersion ellipses we can anticipate assuming it is possible to select the correct steady-current field.

The study plan for the wind field analysis was developed around the idea of taking a detailed look at the wind field during a short, five-day time interval. This approach provided us with good insights regarding the qualitative performance of the model. We found that for the particular conditions of the test, the model did not reproduce the fine-scale features seen in the wind observations. This was particularly true in the region immediately off Port Angeles. We also examined a method of simulating a time history of the wind and found that the arbitrary selection of Race Rocks as a master station was not supported by the data. A principal-component analysis of a portion of the data was performed.

An attempt was also made to reconcile the Evans-Hamilton drifter data (Cox, Ebbesmeyer, and Helseth, 1979) using the combined wind and current fields. The effort was unsuccessful mainly because of the effects of modelling errors. It was possible to detect a current reversal off New Dungeness on 26 August 1978 by calculating the average of the difference between the observed drifter velocities and the model's predicted tidal-current velocities.

SECTION 3

RECOMMENDATIONS

The procedural necessity for making a best-effort analysis of the potential environmental effects of a proposed development has led to the creation of oil-spill models not just for Puget Sound, but for a wide variety of locations. The model examined here is representative, and we believe our conclusions regarding the accuracy of the wind and current simulations have general application. Our primary recommendation is thus that the users of an oil-spill model should be alert to the possible inaccuracies. If the model has been developed for a hydrodynamically complex region such as the one studied here, then one must remain skeptical of any simplistic interpretation of the model's results. In the Strait of Juan de Fuca, for example, the growth over time of the position error exhibits a strong dependency on the slowly varying, baroclinic components of the current; and these current phenomena are not simulated by the model. Thus, the model contributes beneficially to the prediction of a drifter's location only over brief time intervals.

We found that for prediction intervals of of 1 to 5 hours, the model can reduce position uncertainty due to tides by a factor of about two, as compared to predictions using no tidal-current model. During this time, the position uncertainty caused by unknown baroclinic currents is small, but growing, and in the time interval from 5 to 10 hours, uncertainties due to baroclinic currents grow to overwhelming importance. These results are, of course, specific to the region studied, but the principle can be applied to other locations.

Techniques for using the model in an actual spill need to be developed to accommodate these short-comings if the model is to be of any assistance. If the tide model had only very small errors, then in the event of a spill it would be feasible to simply subtract the simulated current from an instantaneously measured current, and so to estimate the important slowly varying component. However, as shown in Table 4, the amplitudes of the model errors are in the range of 10 cm/sec to 30 cm/sec for the important M_2 and K_1 constituents, thus even a 20-cm/sec steady current will be masked by the model error. Nor can we avoid this difficulty by using some other simple scheme to interpolate between the tidal-current reference stations, as demonstrated in Table 3. Therefore, our second recommendation is that additional research be devoted to either improving the accuracy of the interpolation scheme or developing a practicable observational scheme that will allow the determination of the slowly varying currents over short time intervals, such as 1 to 6 hours. Figures 16a and 16b suggest that it might be possible to develop a hybrid system for this purpose based on the use of 20 to 40 drifters coupled with the existing tidal-current model. These drifters should be released on a 2-km grid in the subject area and positions would have to be determined hourly,

irrespective of the visibility. Alternatively, a mobile CODAR with complete data reduction and analysis systems might be developed. A research program of this type is essential if we are to develop any long-term predictive capabilities for use in a spill situation in the Strait of Juan de Fuca or the central basin.

The current subprogram's shortcomings are, of course, caused by its failure to model or otherwise account for the slowly varying baroclinic currents. These currents have only recently been appreciated for their importance to pollutant transport in the region. Topics that might profitably be explored include baroclinic effects on the tides; analytical or numerical simulation of the coastal intrusion phenomena; and further field studies using CODAR and current meter arrays. It would be premature to expect that these studies would immediately lead to an improved modelling capability, but it might be helpful to use modelling as a focus for the work.

The wind field simulation was also found to be rather inaccurate. However, this problem continues to be studied at PMEL as part of the Marine Services program, and progress has been made over the past two years. The wind field simulation model should be updated in the near future to take advantage of this work. There are some difficulties, however, that will require special attention. Foremost is the problem of establishing a suitable statistical framework on which to perform the comparison of observation and simulation. Recent work in nonparametric tests of multivariate processes should be examined to determine whether they can help solve this difficulty (cf. Friedman and Rafsky, 1979). An automated procedure for pattern selection is also required so that statistical comparisons can be made using sufficiently large numbers of samples.

Finally, we must point out that this study has dealt with winds and currents. These parameters, in conjunction with topographical considerations, are undoubtedly the factors that cause oil spill transport. However, the equations that combine these phenomena and produce an oil transport prediction are still little known. It is of vital importance that the direction of future research be compatible with this appreciation of the problem. Specifically, studies of winds and currents should be limited to wind and current phenomena. Combining them in an "oil spill" model seems to be pointless. The requirement that the wind and current models be computerized and of known accuracy should suffice to ensure their ultimate compatibility in an oil spill model.

SECTION 4

TIDAL CURRENT SIMULATION

Three current meter arrays were deployed in the central basin region on July 16, 1978. These stations are referred to as Straits 11, 12, and 13. Each station included a VACM current meter at a depth of 4 m, and each current meter acquired enough data to allow at least a 29-day tidal harmonic analysis. We have used this current meter data as the principal standard for judging the accuracy of our tidal-current simulation routine. The current meter data was obtained from Mr. James Holbrook of the PMEL Coastal Physics Group. It was subsequently analyzed using the R2SPEC computer program which is maintained by Mr. Carl Pearson also of the Coastal Physics Group.

The output of the R2SPEC analysis includes the amplitude, direction of flood (ebb), and phase lag of the various tidal constituents. The analysis is done both in east-west, north-south components, and in terms of components oriented along the major and minor axis of the tidal ellipse. The major axis of this ellipse determines the flood/ebb direction. The major-axis representation of the motion was most suitable for a comparison with the tide model, since the tide model assumes all motions lie along the major axis of the M_2 constituent (Pease, in press).

FUNCTIONAL VALIDATION OF MODEL

Although the model had been extensively debugged and tested in previous projects, the availability of R2SPEC gave us another means of verifying the proper operation of the model. Further, the R2SPEC test was not redundant with earlier efforts to validate the correct functioning of the model. We therefore proceeded with the test.

The model generates its simulated currents by summing as many as three reference station currents, each weighted by a factor lying between 0 and 1.0. The current at the reference station is in turn generated by the summation of the five tidal constituents analyzed and tabulated by Parker (1977). To perform the test we generated (U,V), (east-west, north-south), time series for a 29-day period at the three current meter station locations. The simulated time series at Strait 11 was created with the sum of a .6 weighting on Parker's Station 21 and a .4 weighting on Station 30. The Strait 12 current was generated with the sum of a .3 weighting on Parker's Stations 28 and 42, and a .4 weighting on Station 29. Strait 13 was created with a weighting of .2 on Parker's Stations 31 and 38, and .6 on Station 30. These synthetic currents were then analyzed by R2SPEC, and the amplitude and phase of the five tidal constituents of the simulated tidal currents were determined. Figure 1 shows the location of Straits 11, 12, and 13, and the locations and weights of the reference stations used in the summation.

An alternative method for determining the amplitude and phase at the three stations is, using trigonometry, to determine the amplitude and phase as analytic functions of the weighting factors and the reference stations' amplitudes and phases. This derivation is outlined in appendix A.

The comparison for the 5 tidal constituents used in the model is shown in Table 1. The calculated phase and amplitude, equations (A4a), (A4b), and the equivalent R2SPEC estimates are very similar for the M_2 and O_1 constituents at all three locations, and they are reasonably close for the S_2, N_2, and K_1 constituents. The reason for the slight disagreement in the latter constituent estimates is that R2SPEC includes corrections for errors normally caused by the presence of the host of other tidal constituents. These other constituents are not present in the model's simulated tidal velocity, equation (A5), and so these "corrections" are deleterious. If they were nullified, the analysis would compare even more closely with the calculated phase and amplitudes. In any event, the comparison is sufficiently close to state that the model's simulation of tidal currents accurately reflects the data taken from Parker (1977) and stored in the various arrays. There is no time base error and no indication of transformation errors in going from the major-axis coordinates to east-west, north-south coordinates. We note in passing that the minor-axis velocity estimates from R2SPEC were uniformly zero for all constituents and locations, reflecting exactly the model's simulation process.

ACCURACY OF THE MODEL'S INTERPOLATION SCHEME

We know that the model operates consistently on the data stored in its coefficient arrays. It is not certain, however, whether these coefficients have been selected to create an accurate simulation of tidal currents at an arbitrary point. In order to judge the merits of the model from this second viewpoint, we compared the three model time series with currents observed at Straits 11, 12, and 13. Through a minor communication failure uncovered in the final writing of this report, the model locations for Straits 11 and 12 were taken to be 48°13'N, 126°6'W and 48°20'N, 122°58'W, respectively. These locations are in error by about 2 km from the sites of the July 16th deployment. It was judged that the comparison was still valid, however, since tidal phase, amplitude, and direction of flood change very little over distances as small as 2 km in this area.

Table 2 shows the flood direction, major-axis amplitude, GMT phase, and minor-axis amplitude for the M_2, N_2, S_2, K_1, and O_1 constituents, as estimated from the 29-day records obtained at Straits 11, 12, and 13. Immediately beneath these values are the equivalent parameters as calculated from the simulated time series obtained from the model.

In general, we can see that the model's simulated tidal currents correspond reasonably well with the observed currents. The errors in flood direction range from 1° or 2° to 42°, with a typical value being approximately 10°. The simulated major-axis amplitudes are uniformly low, with the discrepancy ranging from a few cm/sec, to 15 cm/sec in the K_1 constituent at Strait 11. The percentage error of this deficiency ranges from 15% or 20% for the

TABLE 1

A COMPARISON OF A TIDAL ANALYSIS OF MODEL OUTPUT WITH AN ANALYTICAL PREDICTION BASED ON MODEL COEFFICIENTS

		M_2			S_2			N_2			K_1			O_1		
LOCATION		FLOOD DIR °T	amp. cm/sec	Phase Lag (EPOCH,GMT)	FLOOD DIR °T	amp. cm/sec	Phase Lag (EPOCH,GMT)	FLOOD DIR °T	amp. cm/sec	Phase Lag (EPOCH,GMT)	FLOOD DIR °T	amp. cm/sec	Phase lag (EPOCH,GMT)	FLOOD DIR °T	amp. cm/sec	Phase Lag (EPOCH,GMT)
STRAIT 11**	CAL'C'D*	80°	36.7	250.0°	80°	9.0	260.8°	80°	7.4	242.4°	80°	18.1	138.40	80°	15.2	161.5°
	R2SPEC	80°	36.8	248.9°	80°	9.9	251.5°	80°	6.3	248.5°	80°	15.5	119.9°	80°	15.4	164.3°
STRAIT 12***	CAL'C'D*	42°	36.5	311.0°	42°	9.8	332.6°	42°	7.1	301.0°	42°	15.9	205.9°	42°	9.1	182.4°
	R2SPEC	42°	36.1	311.2°	42°	10.8	323.2°	42°	5.9	306.8°	42°	13.7	188.1°	42°	8.9	185.0°
STRAIT 13	CAL'C'D*	95°	33.5	281.3°	95°	8.0	307.6°	95°	6.5	268.7°	95°	15.8	187.5°	95°	9.5	158.5°
	R2SPEC	95°	33.6	281.3°	95°	8.8	298.1°	95°	5.4	274.3°	95°	13.5	169.7	95°	9.3	160.9°
TYPICAL	DIFFERENCE	0°	<1%	<1°	0°	<10%	<10°	0°	<20%	<10°	0°	<20%	<20°	0°	<2%	<3°

* CAL'C'D means the phase and amplitude parameters we calculated from the weighting factors, constituent amplitudes, and constituent phases for the three unique reference stations applicable to the station locations, see Eq. (A4a) and (A4b).

** STRAIT 11 location taken as 48°13'N, 123°6'W

*** STRAIT 12 location taken as 48°20'N, 122°58'W

TABLE 2

A COMPARISON OF SIMULATED TIDAL CURRENTS WITH ACTUAL OBSERVATIONS AT STRAITS 11, 12, AND 13

Station	Location		M_2				N_2				S_2				K_1				O_1			
			°T	Major cm/sec	Epoch GMT	Minor cm/sec	°T	Major cm/sec	Epoch GMT	Minor cm/sec	°T	Major cm/sec	Epoch GMT	Minor cm/sec	°T	Major cm/sec	Epoch GMT	Minor cm/sec	°T	Major cm/sec	Epoch GMT	Minor cm/sec
Strait 11	48°14',123°6'	Observed	92	43.9	296	1.4	89	10.9	265	.6	82	11.5	231	3.8	78	30.3	219	3.3	85	18.2	186	3.3
	48°13',123°6'	Simulated	80	36.8	249	0	80	6.3	249	0	80	9.9	252	0	80	15.5	120	0	80	15.4	164	0
Strait 12	48°21',122°57'	Observed	65	45.6	319	21.9	75	10.6	294	4.4	64	11.0	352	4.2	84	15.4	238	4.1	56	11.9	199	1.7
	48°20',122°58'	Simulated	42	36.6	311	0	42	6.9	307	0	42	10.8	323	0	42	13.7	188	0	42	8.9	185	0
	48°19',122°59'	Parker 29	60	31.2	312	.7	62	6.0	298	1.1	74	9.3	343	3.3	46	16.3	222	3.7	52	11.6	187	.3
Strait 13	48°14',122°57'	Observed	96	41.2	302	8.5	96	8.1	269	.3	109	17.9	252	3.4	109	26.5	225	8.7	105	15.0	178	2.7
	48°14, 122°57'	Simulated	95	33.6	281	0	95	5.4	274	0	95	8.8	298	0	95	13.5	170	0	95	9.3	161	0

M_2, S_2, and O_1 constituents, to 40% or 50% for the N_2 and K_1 constituents. The error in the GMT Epoch value ranges from 5° or 10° to 40° or 50° (with one error of 100° in the K_1 component of Strait 11), but there appears to be no pattern in this error except that the K_1 constituent is uniformly bad. The neglect of the minor-axis velocity in the model leads to errors that are typically 5 cm/sec or less, with the exception of the M_2 component of Strait 12.

A portion of the discrepancy between the observed currents and the model's simulated currents may be due to the differing depths of Parker's reference stations and the current meters we are using for the comparison. Parker's stations vary in depth from 5 m to 22 m, whereas Straits 11, 12, and 13 are at 4 m. Over such a range of depths we know that the direction and amplitude of a tidal constituent can change as a result of baroclinic effects on the tide. Directional changes of 10°-15° and amplitude changes of 5 cm/sec are common in this region in the top 20 m to 30 m. Because there is as yet no known simple, proven method for predicting this discrepancy, we shall ignore it for the present analysis.

It seemed possible that the particular selection of weights is solely accountable for the errors described above. It can be seen from Figure 1 that the Strait 12 position and Parker's Station 29 are close together. Thus, one would think it possible to use Parker's Station 29 as a basis for predicting Strait 12 currents. The consequence of this selection may be seen in Table 2. The major-axis amplitude deficiency is exacerbated in the M_2 and S_2 components, and partially corrected in the remaining constituents. On the other hand, errors in direction of flood are uniformly reduced, and the Epoch values are significantly better for the K_1, S_2, and N_2 components. However, errors still remain, and it appears that we cannot expect to achieve perfection from a simple revision of the coefficent arrays.

The determination of the weighting factors and the station indexing were done manually by the authors of the model in a somewhat subjective way. A simple objective approximation to the process behind the station indexing and weighting is that of a linear interpolation. Are the errors seen at Straits 11, 12, and 13 consistent with this interpretation? If not, can we expect to diminish the errors seen in Table 2 by using a more objective weighting scheme based on linear interpolation between stations?

Table 3 shows the results of a simple analysis of Parker's station data which suggests an answer to these questions. Parker's station locations were studied and eight station triplets were found where all three stations fell nearly on a straight line. The outermost stations were then used to predict the M_2 amplitude and phase of the middle station. The weighting factor applied to a predictor station was simply the fractional distance from the middle station. The distance between the outermost stations varied from 12.6 to 39.6 kilometers, and the weighting factors were typically in the range of .45 to .55, reflecting the fact that the middle station was usually about halfway between the predictor stations. Because the predicted current exhibits an error in both phase and magnitude, we require two measures of

the error. The least ambiguous way to write this error is as the sum of a component that is in phase with the reference signal and a component that lags by 90° Thus:

$$a \cos \sigma t - \hat{a} \cos (\sigma t + \hat{\theta}) = b_1 \cos \sigma t + b_2 \sin \sigma t \qquad (1)$$

where $\hat{a}$ is the linear interpolation estimate of a, and $\hat{\theta}$ is the phase error of the estimate. We do not consider the effect of the statistical uncertainty that clouds our knowledge of the amplitude and the phase of the reference signal, as well as our knowledge of the amplitude and phase of the predictors. Equation (1) may be solved for b_1 and b_2 with the result:

$$b_1 = \hat{a} \cos (\hat{\theta}) - a \qquad (2a)$$

$$b_2 = \hat{a} \sin (\hat{\theta}) \qquad (2b)$$

These b_1 and b_2 values for the eight triplets are shown in Table 3 in the two far-right columns.

The b_1 and b_2 values for the Straits 11, 12, and 13 are also shown in Table 3, and we can see that their range of values is not unlike that seen in the linear interpolation scheme. There is not a sufficient number of data points to allow us the luxury of a statistical test of the hypothesis that the errors of both the model and the linear interpolation scheme are from the same distribution. However, as a practical matter it appears very likely that there is no significant difference between the methods.

TABLE 3

A COMPARISON OF LINEAR INTERPOLATION ERRORS WITH OBSERVED MODEL ERRORS

Reference Station	Predictor Stations St. No.	Wt.	St. No.	Wt.	Dist. (Km)	Reference St. Analysis M_2 Amp cm/sec	M_2 Phase (LT)	Predicted Coefficients M_2 Amp. cm/sec	M_2 Phase (LT)	Error b_1 (inphase) cm/sec	b_2 (90° Lag) cm/sec
4	2	.47	5	.53	38.0	41.8	39°	31.4	63.5	-13.2	13.0
5	4	.51	8	.49	39.6	42.7	61°	43.2	49.8°	-.3	-8.4
7	6	.50	8	.50	13.0	47.3	54°	43.0	62.3°	-4.8	6.2
12	11	.49	14	.51	12.6	72.7	70°	80.5	59.0°	6.3	-15.3
20	16	.39	30	.61	28.2	47.3	74°	41.8	54.1°	-7.8	-13.7
21	22	.44	20	.56	16.7	48.9	67°	54.3	79.1°	4.2	11.4
22	17	.54	26	.46	20.0	63.7	84°	64.5	69.8°	-1.2	-15.8
25	26	.52	78	.48	13.9	67.0	67°	68.6	90.4	-4.0	27.2
Strait 11						43.9	296°*	36.8	249°*	-17.9	25.9
Strait 12						45.6	319°*	36.6	311°*	-9.5	5.1
Strait 13						41.2	302°*	33.5	281°*	-9.5	10.9

*GMT PHASE LAGS

SECTION 5

SIGNIFICANCE OF THE CURRENT MODEL ERRORS

As we have noted, tidal currents created by the model have errors that are a sizable fraction of the observed tidal currents. It is not clear, however, whether these errors are important when viewed in light of the model's intended use. In fact, the problem of what is an "acceptable" error has not been discussed previously. This is a critical deficiency in our thinking on the subject, and to remedy this deficiency, we offer the following analysis both to help critique the existing model and to guide subsequent efforts.

We have found that one parameter useful as an error criterion is the mean squared error in predicted position. This parameter is an indication of the area that ought to be searched if the model is used to locate a drifting object some period of time after it has been released. If this number is small, say on the order of 1 $(km)^2$, then we can go to the location predicted by the model and expect the drifter to be nearby, perhaps within sight of the search vessel. Alternatively, if the number is large, say 100 $(km)^2$, then we should anticipate substantial difficulties in locating the object. Interpreted another way, if we run the model in a simulation mode, then the growth of the mean squared error with time makes it more and more unlikely that a model prediction is a truly representative trajectory. This is particularly true if the trajectory lies near a beach or some other geographic feature that might catch the drifter or channel it into a particular region.

Let us consider three illustrative cases.

Case 1. Trajectory predictions are made with no knowledge of tidal currents, but with perfect knowledge of all nontidal currents.

Case 2. Trajectory predictions are made with no knowledge of the nontidal currents, but with perfect knowledge of the tides.

Case 3. Trajectory predictions are made with the present model with the addition that we have perfect knowledge of the very-low-frequency (weekly and lower) currents.

The first case is unreasonable in any practical sense because it supposes that we have a perfect understanding of wind-driven and baroclinic current phenomena that we are only now learning to identify and categorize and are far from describing in a statistically useful sense. However, this case offers a simplified view of the problem that isolates and helps define the role a tidal-current model plays in trajectory calculations. Specifically, we can use this case to relate errors in tidal-current amplitude and phase to mean squared position errors in locating drifting objects.

CASE 1: No Knowledge of Tides

In addition to perfect knowledge of nontidal currents, we assume for case 1 that amplitude and phase functions are independent of position. We assume also that the trajectory calculation is to begin at a random time. With these qualifications, the displacement due to one tidal constituent is given by the time integration of the velocity. This has a particularly simple form when we are dealing with sinusoidal tidal constituents:

$$D_\ell(\tau_2,\tau_1) = \int_{\tau_1}^{\tau_2} U dt = \int_{\tau_1}^{\tau_2} A_\ell \cos(\sigma_\ell t + \theta_\ell)\, dt,$$

which can also be written as:

$$D_\ell(\tau_0,\xi_\ell) = \frac{A_\ell}{\sigma_\ell} \sin(\sigma_\ell t + \theta_\ell)\Big|_{\tau_1}^{\tau_2} = \frac{A_\ell}{\sigma_\ell}[\sin(\sigma_\ell \tau_0 + \xi_\ell) - \sin(\xi_\ell)] \qquad (3)$$

where

$$\tau_0 = \tau_2 - \tau_1$$

and

$$\xi_\ell = \sigma_\ell \tau_1 + \theta_\ell.$$

Because τ_1 is random, ξ_ℓ is also random. With trigonometry, we can transform equation (3) into the following:

$$D_\ell(\tau_0,\xi_\ell) = \frac{A_\ell}{\sigma_\ell} \sqrt{2}\ (1-\cos\sigma_\ell\tau)^{\frac{1}{2}} \cos(\xi_\ell + \phi) \qquad (4)$$

where

$$\phi = \cos^{-1}\left\{\frac{\sin\sigma_\ell\tau_0}{\sqrt{2}\ (1-\cos\sigma_\ell\tau_o)^{\frac{1}{2}}}\right\}$$

We let

$$\delta_\ell(\tau_o) = \frac{A_\ell}{\sigma_\ell} \sqrt{2}\ \ (1 - \cos\sigma_\ell\tau_0)^{\frac{1}{2}} \qquad (5)$$

and note that this parameter is simply the maximum excursion possible in time period τ_o for a particle being advected by a sinusoidal current. The random phase variate, ξ_ℓ, is uniformly distributed over $(0,2\pi)$.

Based on equation (4), the distribution of $D_\ell(\tau_0)$ is:

$$f_{D_\ell}(D) = \frac{1}{\pi\delta_\ell(\tau_0)\left(1 - \left(\frac{D}{\delta_\ell(\tau_0)}\right)^2\right)^{\frac{1}{2}}}, \quad -\delta_\ell(\tau_o) \le D \le \delta_\ell(\tau_o) \qquad (6)$$

The first two moments of this distribution may be shown to be:

$$E[D_\ell] = 0 \qquad (7)$$

$$\sigma^2_{D_\ell D_\ell} = E[(D_\ell - E[D_\ell])^2] = \tfrac{1}{2}\delta^2_\ell(\tau_0) \qquad (8)$$

The first result (7) is a consequence of the symmetry of equation (6); the second result (8) is the parameter we use to characterize the dispersion of the case 1 assumption.

These results are for the major-axis excursions of one tidal constituent only. If we neglect all minor-axis motions, the displacement of a particle that is acted on by a number of tidal constituents will be given by a summation of the form

$$D(\tau_0) = \sum_{\ell=1}^{M} D_\ell(\tau_0, \xi_\ell) \tag{9}$$

The random phase variates, ξ_ℓ, are related to one another by the starting time, τ_1, via the modulo operation,

$$\xi_k = \text{mod } (\sigma_k \tau_1 + \theta_k, 2\pi) \tag{10}$$

There is some uncertainty on our part as to the nature of the statistical relationships that exist between the random phase variates defined by (10). On one hand, equation (10) is somewhat analogous to computer algorithms that generate random numbers. On this basis, we believe that an argument could be made that the phases are statistically independent provided the frequencies in (10) are incommensurate. Unfortunately we know that the frequencies selected to represent tidal phenomena are not independent, and that there are a number of simple relationships that link them. For example, the sum of the O_1 and K_1 frequencies exactly equals the M_2 frequency. These linkages result in characteristic tidal waveforms. In Seattle, for example, the M_2, O_1, and K_1 tides often combine so that consecutive diurnal high waters are of nearly equal magnitude while the intervening low waters are of much different size. Because of the linkage in frequencies, the opposite pattern occurs only rarely. So from this standpoint, the phase variates are to be expected to have some very complicated, multidimensional, statistical dependencies. We have not been able to resolve this problem, so we have opted to assume that the phase variates for the different tidal constituents are independent.

The importance of this assumed independence is that we may use the central limit theorem (CLT) to deduce the approximate form of the distribution of $D(\tau_0)$. The simplest form of the CLT says that the sum of n independent, identically distributed, random variates with finite mean and variance converges to a normal (or Gaussian) distribution in the limit as n goes to infinity. The theorem also holds for variates distributed according to a scale factor transformation of a common distrubution function. Equation (6) is of this type with $\delta(\tau_0)$ being the scale factor.

It is well known that the percentile ranges of a normal distribution are related to the square root of the variance, the standard deviation. Thus, if σ^2_{xx} is the variance of the distribution on x, then 68% of the distribution lies within $\pm\ \sigma_{xx}$ and 95% lies between $\pm\ 2\sigma_{xx}$. In analogy, and with reference to the CLT, we should expect the variance of our summed variate to be functionally related to the percentiles of that distribution. Because the distributions of the summands have square-root singularities at the extremes of their range, and because the number of summands is small (only five), the CLT

provides only a rough approximation to the actual distribution of the summed variate $D(\tau_0)$. Thus, we cannot be certain that precisely 68% of our observations will fall within one standard deviation of the mean. However, experience with the CLT suggests that the bulk of the observations will fall within one standard deviation, and it is in this loose sense that we assert that the standard deviation is related to a "characteristic" error of position. Reiterating, we assume that the summands are independent, thus the summed variate $D(\tau_0)$ will be distributed in an approximately Gaussian form, and this allows us to put a frequency interpretation on the standard deviation that supports our contention that the standard deviation of $D(\tau_0)$ is an appropriate measure of dispersion. Given the standard deviation as the radius of the circle of dispersion, the variance is thus proportional to the area in which the drifting object is likely to be found.

Also because of the assumed independence of the summed variates, the variance of the sum may be related to the variances of the summands, equation (8). This follows because of the well-known result that the variance of the distribution of the sum of two independent random variables is given by the sum of the variances of the summands,

$$\sigma_{ss}^2 = \sigma_{xx}^2 + \sigma_{yy}^2 ,$$

where $s = x + y$.

This result is exact and not dependent on the CLT approximation. Thus, extending this result to five summands and applying it to our problem,

$$\sigma_{DD}^2 = \sum_{\ell=1}^{5} \tfrac{1}{2}\delta_\ell^2(\tau_0) = \sum_{\ell=1}^{5} \left(\frac{A_\ell}{\sigma_\ell}\right)^2 (1 - \cos\sigma_\ell\tau_0) \qquad (11a)$$

This completes our argument that the standard deviation (the square root of the variance) of $D(\tau_0)$ provides a useful and readily calculated geometric measure of the dispersion.

Case 1 assumes we make our predictions with no knowledge of the tidal currents. We interpret this to mean that the major axis of tidal-current motion has no favored angular orientation. Under the assumption that all five tidal constituents share a common major axis, the radius of dispersion is determined from the square root of (11a):

$$R(\tau_0) = \left(\sum_{\ell=1}^{5} \left(\frac{A_\ell}{\sigma_\ell}\right)^2 (1 - \cos\sigma_\ell\tau_0) \right)^{\frac{1}{2}} \qquad (11b)$$

Figure 2 shows this $R(\tau_0)$ variate at Straits 11, 12, and 13. The amplitude values used in the presentation are taken from the July 16th analysis (see Table 2). The circumference of the circle of dispersion is shown at hourly intervals for τ_0 varying from 1 to 12 hours. This half-day limitation on the use of equation (11b) has been chosen so as to accommodate the restrictions that are implicit in our assumption that the phase and amplitude

parameters are constant with respect to displacement. In an actual realization, as a particle is transported away from the release point, the amplitude and phase parameters will change. To illustrate this advection effect, we have sketched the dispersion circle about mean-flow streamlines taken from the CODAR data over the period 23 to 25 August 1978. Notice that the dispersion curve from Strait 13 encompasses the Strait 11 site at hours 5 through 12. Particles advected into the vicinity of Strait 11 would no longer have tidal amplitudes and phases like those at Strait 13 which was their release site, but rather would behave like particles released at Strait 11. These effects would play an important and perhaps dominant role in long-term tidal displacement calculations.

Figures 19 and 20 of Parker (1977) show that the M_2 and K_1 tidal ellipses are nearly always in close alignment in this region. Thus the assumption of a shared major axis is not a bad one. It is possible, however, to calculate the variance of the distribution of a sum of random variates in which each tidal current variate can assume an arbitrary spatial orientation with respect to a reference axis. That is,

$$D(\tau_0) = \sum_{\ell=1}^{5} \delta_\ell(\tau_0)\cos\phi_\ell \cos(\xi_\ell + d)$$

where ϕ_ℓ is the angle between the reference axis and the variate's major axis. We assume that ϕ_ℓ is a uniformly distributed random variate with range $(0,2\pi)$ and we continue to neglect motions in the minor axis direction. Under these assumptions, the result analogous to (8) is:

$$\sigma^2_{D_\ell D_\ell} = .2865\ \delta^2_\ell(\tau_0)\ , \tag{12a}$$

and

$$\sigma^2_{DD} = \sum_{\ell=1}^{5} (.573)\delta^2_\ell(\tau_0) \tag{12b}$$

(See appendix B.)

Thus if tidal-current constituents were directed in this random fashion, we would only reduce the standard deviation by a factor of $\sqrt{.573}$, or about .75. In short, the assumption that the various constituents act along the same axis is both reasonable and uncritical.

In terms of our assumptions, Figure 2 can be interpreted as depicting the circular area one would search in order to find a drifting object whose average drift was known assuming nothing was known about the tides. In practical terms, these circles are much too large in the cross-channel direction since the local geography strongly channels the flow. Thus these curves should not be used for any purpose other than to explore the consequences of our assumption of complete ignorance of the tides.

TABLE 4

TIDAL CONSTITUENT ANALYSIS OF MODEL ERRORS

STATION	Constituent	Major Amp. (cm/sec)	Minor Amp. (cm/sec)	Flood Dir. (°T)	Model Dir (°T)
STRAIT 11	M_2	30.5	1.9	84	80
	N_2	9.7	1.0	111	
	S_2	6.3	4.4	18	
	K_1	4.6	2.6	58	
	O_1	28.1	.9	79	
STRAIT 12	M_2	9.6	1.1	90	42
	N_2	1.8	.9	148	
	S_2	3.8	1.0	112	
	K_1	1.8	.3	84	
	O_1	6.8	1.8	119	
STRAIT 13	M_2	28.9	.3	98	95
	N_2	13.7	2.2	125	
	S_2	2.1	.3	155	
	K_1	8.8	.9	98	
	O_1	17.5	5.8	116	

Although the assumptions of case 1 are too coarse to provide a practical guide to the dispersion problem, they are simple to understand, and therefore they serve a useful conceptual purpose. Moreover, case 1 lays the foundation for an interesting comparison between the no-knowledge conditions of case 1 and the uncertain knowledge situation we face when using the tidal-current model. In this real-life situation, errors in trajectory position will be caused by inaccuracies in the model's tidal current simulation, as well as by phenomena not included in the model. The analysis above may be used to estimate the relationship between the tidal-current errors and the error in predicted position. Table 4 shows the R2SPEC analysis of the tidal-current signal formed from the difference between the observed tidal currents and the simulated currents. We consider these difference currents to be random errors associated with the model's predictions. The source of these error signals can be traced back to the phase and amplitude errors of Table 2 already discussed, and to the error in the alignment of the major, or flood, axis. Further, these errors are augmented by the model's explicit neglect of the minor-axis tidal velocities.

The last column in Table 4 shows the tidal-current flood direction specified in the model. Notice in the Strait 12 simulation that both the major-axis amplitude errors are small, and the direction of the difference velocity's flood is randomly scattered relative to the model's flood direction. This scattering in the difference velocity flood direction is what we expect if the model had no systematic errors. As we can readily see from either Table 2 or the correlation of the difference velocity flood direction and the simulated velocity flood direction in Table 4, some sort of systematic error is present in the model's simulation of the Straits 11 and 13 velocities. Nevertheless, the uniform scattering assumption provides a useful tool for analyzing errors associated with the model.

Figure 3 shows the dispersion associated with tidal-constituent errors of Table 4 under the assumption that the major axis of motion is randomly oriented. The diagram is rigorously correct only for Strait 12, but the features of the dispersion envelopes of Straits 11 and 13 are qualitatively correct if we allow for a moderate (up to 33%) elongation of the circles in the flood direction, and an equally sizeable reduction in the direction perpendicular to the flood. This diagram illustrates the contribution that the model makes to reducing uncertainty in the predicted position of a drifting object, assuming all nontidal currents are known exactly. At best, and after a few hours, the model predicts the location to within about 1 km at Strait 12. At Strait 13, the radius of the circle of uncertainty is about 3 km after 5 hours, and at Strait 11 the radius is about 4.5 km after 5 hours. This corresponds to a reduction in search area of 90%-95% at Strait 12, and (perhaps) 50% at Straits 11 and 13.

CASE 2

Case 2 is the converse of case 1. We now assume that drifter position predictions are made in ignorance of all nontidal motions, but with complete knowledge of the tidal currents. Again we are forced to limit the duration of the trajectory prediction to small times, say 12 hours, to prevent out-running our localized knowledge.

Unlike the tidal currents, the physical mechanisms behind the nontidal currents are diverse and poorly documented. The simplest way to categorize these motions is in terms of the manner in which they appear in our current observations. One class of motion has periods shorter than one hundred hours, and these motions can be resolved as frequency components in Fourier analyses of the current records now available. As a general rule, these motions are weak; a typical root-mean-square amplitude for all the motions falling in the frequency band between the daily and semidaily tides is only 3 or 4 cm/sec. The other class of motion is comprised of the long period oscillations that appear as mean values in our 15- and 29-day current observations. These motions are not truely steady currents. In all likelihood, these slowly varying currents are associated with changes in the density structure of the region. The density structure is principally dependent upon fresh-water runoff from the Fraser River and also from the onshore advection of low-density surface waters by winds acting on the region lying west of the coast of the state of Washington. These motions are generally of large amplitude, and the intrusions of low-density surface lenses have a sporadic appearance in the current records.

The estuarine runoff is perhaps the most predictable feature of the region, and in the Strait of Juan de Fuca at midchannel, the average outflowing current varies from a minimum value of 10 cm/sec to 30 cm/sec in late winter to a high of 30 cm/sec to 40 cm/sec in late summer (Cannon, 1978, Figure 27). This flow is also seen in CTD sections across the Strait and in satellite images of surface-water properties. Superimposed on this outward flow are intrusions of low-density lenses of water advected to the mouth of the Strait by winds acting offshore. These intrusions may occur rather frequently, and they can result in eastwardly (up-channel) flow along the south shore of the Strait of Juan de Fuca with speeds of up to 50 cm/sec and durations of many days. The CODAR images of the Port Angeles region on 26 August 1978 document the complex behavior of the upstream front of one of these intrusions (Frisch, Holbrook, and Ages, 1980).

The dispersion caused by the weak, high-frequency motions that are resolved in our current records may be estimated using a procedure that is entirely analogous to that used on the tides in case 1. We group the current speed energy in the various frequency bands into five discrete frequencies and model these motions as though each discrete frequency was the equivalent of a tidal constituent in case 1. Table 5 shows the parameters we have used for this representation of the nontidal motions. The values in this table reflect a Fourier analysis of the kinetic energy at Straits 11, 12, and 13 as seen in the 16 July 1978 deployment (Holbrook, personal communication).* We assume for this case that the orientation of this motion is random and so use equation (12b) to calculate the variance of the drift position. Figure 4 shows the dispersion envelopes for these representations. Notice that the error associated with the neglect of these motions is a very small fraction of the case 1 error, and that it is comparable with the tide model dispersion envelope at Strait 12 (Figure 3). These currents are probably caused by the oscillating wind stress that acts on the region. These stresses result in highly localized surface boundary layers, and in weak barotropic current

* Mr. J. R. Holbrook, NOAA/PMEL, Seattle, Washington.

TABLE 5

PARAMETERS FOR THE DISCRETE FREQUENCY SIMULATION OF THE NONTIDAL OSCILLATORY CURRENTS

Freq. Band (cyc/hr)	Center Freq. rad/hr	Amplitude of Discrete Sinusoid (cm/sec)		
		Strait 11	Strait 12	Strait 13
.008 - .016	.075	2.2	2.2	2.0
.016 - .024	.125	2.2	2.2	2.0
.024 - .032	.176	2.2	2.2	2.0
.05 - .07	.377	3.5	3.5	3.2
.09 - .2	.911	8.1	8.1	7.4

fields that extend over the whole region. It is reasonable to consider these motions omnidirectional.

Figure 5 depicts the magnitude and direction of the average current observed at a number of locations within the central basin and Strait of Juan de Fuca regions. These vectors are taken from Figure 38 of Cannon (1978). With the exception of six vectors taken from the mouths of Rosario and Haro Straits, which show a uniform out-strait flow, the remainder are widely scattered and show no obvious channeling. These averages are the net flow seen over various periods ranging from 10 to 30 days, and we reiterate that they are not good estimates of the true average because of this relatively short record length.

Although these vectors are not good estimates of the true, statistical, average current, it is reasonable to presume that they are representative of the net current one might encounter in any given drifter experiment. The vectors themselves come from many different locations, and it would make no sense to try to combine these values in an elaborate statistical model. We therefore limit our analysis to the simple determination of the average magnitudes of the observed net current and let this value characterize the random, net drift we should expect in a drifter experiment. This average was found to be .66 km/hour.

Figure 6 shows three groups of concentric circles centered on Straits 11, 12, and 13 respectively. These circles depict the hourly transport caused by an average drift of .66 km/hour. The circular geometry reflects our uncertainty in determining the direction of the net drift. These circles are to be interpreted as a characteristic transport distance. If there were no tidal currents or other motions, and if the streamlines were straight, then a drifter would, on the average, be located somewhere on the circumference of one of these circles. Figure 4 and Figure 6 are the counterpart to Figure 2. A comparison of Figure 4 and Figure 6 shows that the very-low-frequency, density-related motions depicted in Figure 6 are the critical elements in the case 2 problem.

A comparison of the area of the 12-hour envelope of the net drift portion of case-2 to the case-1 envelope (which encompasses all position errors from the release to hour 12), shows them to be of comparable size. A better com-

parison is to plot the radius of the position error as a function of time for the two cases. This is done in Figure 7, where we can see that the error associated with complete ignorance of the tides (case 1) is somewhat greater than the error caused by ignorance of the nontidal currents, for trajectory durations less than 10 hours. After that time, the case 2 current errors become dominant. The contribution of the high-frequency, nontidal oscillations in this figure can be seen to be of only modest importance.

CASE 3: Existing Model with Assumed Steady Current

The uncertainty in position due to our ignorance of the very-low-frequency currents (Figure 6) is so great as to require the adoption of some hypothesis regarding the behavior of these currents. The alternative, the treatment of these currents as a simple random process, results in a region of uncertainty that is so large as to obscure whatever insights the tidal-current model might provide. This is not a novel observation. In a previous study of oil spill trajectories in the region (Stewart, 1978), the results were framed in light of the contrast between a no-steady-current hypothesis and a uniform, ebb-directed, steady-current hypothesis. The necessity for such an assumption that is provided by Figure 6 is simply another way of arguing the same point.

The case 3 assumptions are that we know these long-period currents. The purpose of this analysis is to outline the region of uncertainty associated with the use of our model in such a situation. There are two ways we can proceed. We can combine our previous analytical results, principally Figures 3 and 4, or we can integrate the differences between the observed current velocities of the simulated current velocities to estimate the time behavior of the error. We have adopted the latter method because it is less dependent on the many assumptions required by the analytical method, and because it will serve as a check on our previous calculations.

Three difference-current time series were created and then divided into 48-hour intervals. An initial time was randomly selected within each interval. We then integrated the difference velocity for durations of 1, 3, or 10 hours to determine one realization of the error growth. Using distinct 48-hour intervals, we acquired between 20 and 30 independent realizations for each of the three durations, at all three stations. The resultant (x, y) positions were then analyzed to determine the variance-covariance matrix, and the coordinates of the ellipse containing 68% of the observations were then calculated assuming the (x, y) variates were drawn from a bivariate normal distribution. This ellipse was compared with the scatter plot to ensure qualitative agreement with the data.

Figure 8 depicts these ellipses for Straits 11, 12, and 13 at durations of 1, 3, and 10 hours. The steady flow used in creating these figures was taken from the net flow in the current meter observation. Notice that Straits 11 and 13 have flows consistent with the CODAR streamlines used in our previous representations, but the net flow at Strait 12 is oriented in the opposite direction. This graphically illustrates the importance of the slowly varying currents, and it gives warning of the dangers in assuming knowledge of this phenomenon.

SECTION 6

WIND FIELD SIMULATION

The wind field in the region is modeled using a time series of hourly wind velocity observations at a master station and a large-scale wind pattern that extrapolates the wind velocity to areas that are distant from the master station. The wind pattern is determined using a numerical model that calculates the winds that would result from the application of a steady pressure gradient across the region (Overland, Hitchman, and Han, 1980). This submodel accounts for the topographic channeling of the dense marine boundary layer. The spatial resolution of the program is such that the major features of the Olympic Mountain Range are discernable, but hills such as those that are seen in the city of Seattle do not appear. The cost of computing these regional wind patterns is great, and so the model uses a library of 8 patterns, each selected to represent a characteristic pressure gradient condition. A sequence of pattern types is selected for the period of the master station wind velocity observations, based on the evolution of the regional pressure gradient. This is presently a tedious and somewhat subjective manual task. The wind simulation is thus based on empirical observations, but the interpolation/extrapolation junction is determined objectively from a physically based numerical model. In this respect the wind model differs from the tidal-current model in which the interpolation methods were based on manually determined coefficients of uncertain underpinning.

Some numerical algorithm is required to combine the wind patterns and master station observations. Stewart (1978), in an oil-spill study using the MESA-Puget Sound model, developed a technique wherein a scaled and rotated hourly difference velocity was applied throughout the region. This technique caused the simulated velocity at the master station to equal the observed velocity, and at surrounding points the simulated velocity changed in amplitude and direction in a fashion determined by the wind pattern. A characteristic of this method of extrapolating the observed velocity is that if the pattern velocity equals the observed velocity, then the pattern velocity is applied unperturbed throughout the region.

The purpose of this algorithm was twofold. First it caused the simulated wind field to vary hourly. These high-frequency variations would not be present in the simulation if the wind field had been created by using a sequence of patterns. Secondly, the algorithm assured agreement between the simulated and observed winds at the master station.

A complete evaluation of the wind field simulation should be based on an examination of both the patterns and the algorithm used to turn these patterns into extrapolation and interpolation functions. However, for this study, we have judged it sufficient to examine just the characteristics of the patterns.

We have taken this course because Stewart's algorithm was selected largely on subjective grounds, and whatever merit the algorithm might have, it is predicated on the assumed agreement between the model's wind patterns and the observed winds. If the patterns are a poor fit to the data, then any agreement between the algorithm's velocities and the observations would be purely fortuitous. Little would be learned if the fit was less than perfect. Further, an examination of the pattern errors should uncover any simple method for perturbing the wind patterns so as to achieve the purposes of the extrapolation algorithm.

Because the determination of the pattern sequence for an extended period is a laborious task, we decided to closely examine the wind field simulation over a short time interval. To be compatible with the analysis of the joint experiment data, the period 22-26 August 1978 was selected. Large scale isobaric weather maps and the hourly wind observations at Race Rocks were obtained and given to the wind model's creator, Dr. James E. Overland of PMEL, who determined a pattern sequence based on 6-hour pattern intervals. The period selected for study turned out to have rather anomalous weather for the summer months, but we judged it to be as fair a test as any other that might be devised around a five day period. The pattern sequence for this period was determined to be:

6,5,5,5,5,2,2,3,3,3,3,4,4,5,5,3,3,4,4,4

where the integer serves as an index to the pattern type. It can be seen that the bulk of the interval was accounted for by patterns 3, 4, and 5. These patterns correspond to pressure gradients such that the large scale, extra-regional flow is from the south, southwest, and west respectively. Figures 9, 10, and 11 show the regional wind fields for these cases.

To see whether there is a basis for separating the time series into segments, we performed a principal component analysis of the wind observations from Smith Island, New Dungeness, Race Rocks, and Tatoosh Island. These locations are shown in Figure 12. This analysis revealed that 42% of the variance observed at the four stations could be accounted for by perturbations to the mean wind speed that would simultaneously lie to the east-northeast at Tatoosh, south at Race Rocks, west-northwest at New Dungeness, and north-northwest at Smith Island. The mean wind velocity and these perturbations are shown in Figure 13a. This result may be interpreted as follows. Under conditions that would cause the wind at Tatoosh to become more southerly (in the meteorological sense), the wind at Smith Island would swing a little to the east, the wind at Race Rocks would swing to the north from its mean northwesterly direction, and the wind at New Dungeness would swing to the southeast from its mean southerly value.

The second principal component is depicted in Figure 13b, and it accounts for 18% of the observed variance. Notice that positive perturbations to this component will partially cancel positive perturbations to the first principal component at Tatoosh and Smith Islands, while enhancing the northerly and easterly swings at Race Rocks and New Dungeness respectively. Alternatively, if the second component is given a positive perturbation while the first component is negatively perturbed, then the Race Rocks and New Dungeness

velocities would tend to remain constant while the wind at Smith Island would drop and swing south, and the wind at Tatoosh would drop and swing to the east. The third principal component accounted for 14% of the variance, and it is the last significant descriptor of the data, the remaining, smaller components accounting for 9%, 7%, 6%, 3%, and 1% of the variance respectively. This component is shown in Figure 13c. Whereas the first two principal components caused variations of approximately equal size at all four locations, this third component is effective mostly at the two eastern-most stations, Smith Island and New Dungeness. It can be seen that negative amplitudes applied to this component will result in a westerly rotation and increase in wind speed at Smith Island, and a calming at New Dungeness. The wind at Race Rocks simultaneously increases and swings to the north. This third component thus represents some kind of eddy in the lee of the Olympic Mountains.

An obvious question is whether these components are related to the pattern sequences. Figure 14 shows the amplitudes of these three components at three hourly intervals. The three plots, W_2 vs W_1, W_3 vs W_1, and W_3 vs W_2, are two-dimensional plan views of the three dimensional (W_1, W_2, W_3) space. That is, any given wind velocity observation can be approximated by a summation of the three principal components with weights W_1, W_2 and W_3. The (W_1, W_2, W_3) space thus provides a means of representing the observations. The bulk of the observations form a cluster in the vicinity of the origin, with a slightly negative average value for the W_2 component. However, the large amplitude observations tend to fall into two groups. Observations that were made during Pattern 3 intervals have positive weights on the first component and negative weights on the second and third. This results in an increasing southerly wind at Tatoosh and Smith Islands, a southerly wind at New Dungeness that drops and swings to the east, and a north-northwest wind at Race Rocks that increases slightly. Behavior of this type would seem to fall somewhere in between Patterns 3 and 4 and is not well represented by either (see Figures 9 and 10).

Observations made during Pattern 4 and Pattern 5 intervals, that had large negative weights on the first component, had large positive weights on the second component and negative weights on the third. This corresponds to an easterly swing at Tatoosh, a westerly swing at Race Rocks, a slight drop at New Dungeness, and a slight westerly swing at Smith Island. The Tatoosh behavior does not correspond to either Pattern 4 or 5. The New Dungeness behavior seems more characteristic of Pattern 4 than Pattern 5, and yet Pattern 5 intervals had the extreme weights in this cluster.

Another way of looking at the data is to draw a wind velocity scatter diagram for each pattern type at several stations. Focusing now on the central basin, Figure 15 shows the wind velocity clusters at Smith Island, Point Wilson, New Dungeness, and Race Rocks. Notice that the Pattern 3 data clusters nicely at Smith Island and Point Wilson. It is rather scattered at Race Rocks and strongly bimodal at New Dungeness, with the predicted wind rather too easterly for the large amplitude cluster. Wind Pattern 4 correctly places the wind velocity at New Dungeness at calm. Other stations tend to be rather scattered, although the model predictions are indicative of the predominant quadrant. Wind Pattern 5 does a poor job of sorting or predicting the tendency of the Smith Island, New Dungeness, and Point Wilson observations, but

it picks up one mode of what appears to be a bimodal distribution at Race Rocks.

These observations are too limited in number to warrant further statistical analysis. However, they do suggest some general conclusions. First, there appears to be a strong eddylike motion between Race Rocks and New Dungeness. This motion apparently results from extraregional flows that fall somewhere between the Pattern 4 and Pattern 5 boundary condition. Further, the bimodal behavior of the wind at Race Rocks and New Dungeness suggests that there is some threshold value of pressure gradient below which light and variable winds prevail. Once this threshold is exceeded, the model's predictions are somewhat more reliable, but still subject to relatively large errors in direction. The behavior of the wind at Tatoosh under Pattern 4 and 5 conditions is paradoxical, but perhaps this simply reflects the importance of sub-grid-scale topography on local winds.

The fundamental precept of the wind model is that a substantial fraction of the regional wind patterns can be represented using a library containing a fairly small number of patterns based on time-steady pressure gradients. This assumption is critical, and it requires a great deal more study. In the five-day period we examined, the principal component analysis of the wind observations at four stations determined that 74% of the variance could be accounted for by using three wind patterns. Unfortunately the three patterns determined from the model did not show much agreement with the principal component patterns.

Another important point that can be made regarding the wind field simulation is the importance of matching the master station selection with the wind field behavior. None of the stations that we examined had uniformly good agreement with the three pattern types that occurred during the observation interval. For example, only one Race Rocks observation in Pattern 3 intervals fell within ten degrees of the predicted wind. By using Race Rocks as a master station for Pattern 3 winds, we essentially negated the good fit seen at the other three stations (Figure 15), since a large error velocity would be determined from the difference between the Race Rocks observations and the model predictions, and this error would then be applied to the other stations.

More generally, the selection of an algorithm for combining observed winds and the regional patterns appears to be a difficult problem. If the wind field actually has a threshold for its response to the large-scale pressure gradient, as suggested by the histograms at Race Rocks and New Dungeness, then the algorithm will have to create very small-scale, weak winds for conditions below the threshold, coupled with patternlike winds once the threshold is exceeded. The statistical properties of the sub-threshold local winds will have to be studied to determine spatial coherence scales and the characteristics of the time variability.

SIGNIFICANCE OF WIND MODEL ERRORS

Because of the limited amount of data and the subsequently qualitative nature of the analysis, there is no reasonable method for estimating in a statistical sense the magnitude of the simulated wind velocity errors. Thus,

even if we postulated a formula relating wind and drifter velocities, it would not be possible to make quantitative estimates of the dispersion caused by the model errors. However, it is possible to draw some conclusions regarding the adequacy of the simulation method.

To use the model in its present state, with its limited pattern repertoire, is to chance misestimating the wind by 45° to 180° in certain key regions. The area off Port Angeles is one such region when the extraregional wind is from the south to southwest. The model predictions could be in error by 180°; and with a 3% wind drift factor, the resultant drift could easily be in error by 15 cm/sec to 30 cm/sec, or an amount equivalent to the steady baroclinic currents.

SECTION 7

DRIFTER RESPONSE STUDIES

When we first proposed this work, we envisioned an analysis of the Cox, Ebbesmeyer and Helseth (1979) drifter data. This study was to reveal the response of drifters to surface winds, and it was to be the subject of a separate report. Because of the relatively large errors in the tidal-current and wind models, the proposed analysis was not successful. Although this work may seem somewhat tangential to the present report, it does provide further insight into the importance of the model errors. Certainly, any model that cannot make good hindcasts must be of questionable validity in the forecast mode.

The results of this failed investigation are important also because they bear on the concept of the oil-spill-of-opportunity research program, one task of which was to infer the transport equations for oil slicks from data acquired in actual oil spills. In contrast to most oil spill investigations, we had the benefit of many current meter and anemometer records, we had good data on the positions of easily recognized drifters, and we had our computer model with which to perform the various calculations and interpolations. The fact that our analysis was inconclusive despite all these advantages ought to be considered in the design of any future spill-of-opportunity experiments.

The drifter data were taken from the Plates in Cox, Ebbesmeyer, and Helseth (1979). This data consisted of the position of 97 drift sheets deployed over the period 22-26 August 1978. Positions were determined by aircraft overflying the sheets, and the error in position was estimated by Cox et al., at 31 meters. The data were acquired only during daylight hours and the time between fixes was nominally about 30 minutes. Using the known position, we determined the average velocity by dividing the distance traveled by the time between fixes. This velocity was applied at the midpoint between the known positions. If the time interval exceeded two hours, the point was cast out.

We then sorted the data by day and by location. The latter sorting was based on a nearly square grid in which the north-south cell dimension was 2 minutes of latitude and the east-west cell dimension was 3 minutes of longitude. This corresponds to a square about 3.6 km on a side. This data set was then examined, and grid squares that over the five-day experiment had fewer than ten distinct drifters were combined with adjacent squares to form a cell with sufficient data to allow statistical treatment.

Because the wind model had proven itself unreliable in this area, we decided to use the observed winds at Race Rocks and at New Dungeness for the estimate of the surface wind. The wind data from Race Rocks and New Dungeness

were stored in our data arrays at hourly intervals. The hourly value at New Dungeness was the average of three readings taken at twenty-minute intervals centered on the hour. The drifter velocities, however, were determined at irregular times as dictated by the times of the position fixes. To accommodate this problem, the wind was linearly interpolated from its hourly value to the time of the drifter velocity determination. In this interpolation, we might have done better at New Dungeness had we used the original, twenty-minute wind records.

Several data files were then created containing the interpolated wind velocities and a residual velocity equal to the difference of the drifter velocity and the tidal-current velocity as determined by the model. These data files were then analyzed to see if there was any statistical basis to support a drift equation of this general form:

$$\begin{bmatrix} u_d \\ v_d \end{bmatrix} = \alpha' * \begin{bmatrix} \cos\theta' & -\sin\theta' \\ \sin\theta' & \cos\theta' \end{bmatrix} \begin{bmatrix} u_\ell \\ v_\ell \end{bmatrix} + \begin{bmatrix} u_t \\ v_t \end{bmatrix} + \begin{bmatrix} u_s \\ v_s \end{bmatrix} + \begin{bmatrix} \varepsilon^1 \\ \varepsilon_2 \end{bmatrix} \tag{13}$$

where (u_d, v_d) is the drifter velocity, (u_ℓ, v_ℓ) is the local wind velocity, (u_t, v_t) is the tidal current velocity, (u_s, v_s) is the slowly varying baroclinic current velocity, θ' is an angle of rotation between the local surface wind and the motion it induces at the surface, and ε_1 and ε_2 are random measurement errors. Since we used a shore-based station to estimate the local winds, we must also include a possible rotation and amplification of the shore station wind. That is, in any given grid cell,

$$\begin{bmatrix} u_\ell \\ v_\ell \end{bmatrix} = \alpha'' \begin{bmatrix} \cos\theta'' & -\sin\theta'' \\ \sin\alpha'' & \cos\alpha'' \end{bmatrix} \begin{bmatrix} u_w \\ v_w \end{bmatrix} \tag{14}$$

Thus the complete model is:

$$\begin{bmatrix} u_\ell \\ v_\ell \end{bmatrix} = \alpha \begin{bmatrix} \cos\theta & -\sin\theta \\ \sin\theta & \cos\theta \end{bmatrix} \begin{bmatrix} u_w \\ v_w \end{bmatrix} + \begin{bmatrix} u_t \\ v_t \end{bmatrix} + \begin{bmatrix} u_s \\ v_s \end{bmatrix} + \begin{bmatrix} \varepsilon_1 \\ \varepsilon_2 \end{bmatrix} \tag{15}$$

where $\alpha = \alpha' * \alpha''$, $\theta = \theta' + \theta''$.

Let (u_t', v_t') be the tidal currents predicted by the model, so $\vec{u}_R = \vec{u}_\ell - \vec{u}_T'$. The (u_R, v_R, u_w, v_w) covariance matrix is then given by:

$$\sigma^2_{u_R u_R} = \alpha^2 \cos^2\theta\, \sigma^2_{u_w u_w} - 2 \sin\theta \cos\theta\, \sigma^2_{u_w v_w} + \sin^2\theta\, \sigma^2_{v_w v_w} + \sigma^2_{\varepsilon\varepsilon} \tag{16a}$$

$$\sigma^2_{v_R v_R} = \alpha^2 \sin^2\theta\, \sigma^2_{u_w u_w} + 2 \sin\theta \cos\sigma^2_{u_w v_w} + \cos^2\theta\, \sigma^2_{v_w v_w} + \sigma^2_{\varepsilon\varepsilon} \tag{16b}$$

$$\sigma^2_{u_R v_R} = \alpha^2 \cos\theta \sin\theta \,(\sigma^2_{u_w u_w} - \sigma^2_{v_w v_w}) + \sigma^2_{u_w v_w}(\cos^2\theta - \sin^2\theta) \qquad (16c)$$

$$\sigma^2_{u_R u_w} = \alpha \cos\theta\, \sigma^2_{u_w u_w} - \alpha \sin\theta\, \sigma^2_{u_w v_w} \qquad (16d)$$

$$\sigma^2_{u_R v_w} = \alpha \cos\theta\, \sigma^2_{u_w v_w} - \alpha \sin\theta\, \sigma^2_{v_w v_w} \qquad (16e)$$

$$\sigma^2_{v\, u_w} = \alpha \cos\theta\, \sigma^2_{u_w v_w} + \alpha \sin\theta\, \sigma^2_{u_w u_w} \qquad (16f)$$

$$\sigma^2_{v\, v_w} = \alpha \cos\theta\, \sigma^2_{v_w v_w} + \alpha \sin\theta\, \sigma^2_{u_w v_w} \qquad (16g)$$

provided $\vec{u}_T - \vec{u}'_T$ is neglible. Here (u_w, v_w) is assumed the independent variable, and we assume

$$\sigma^2_{\varepsilon_1\varepsilon_1} = \sigma^2_{\varepsilon_2\varepsilon_2} = \sigma^2_{\varepsilon\,\varepsilon}\,, \quad \sigma^2_{\varepsilon_1\varepsilon_2} = 0.$$

In addition to the seven conditions of equation (16), we may also show that $\alpha^2 > 0$, $\sigma^2_{u_R u_R} > \sigma^2_{\varepsilon\varepsilon}$ and $\sigma^2_{v_R v_R} > \sigma^2_{\varepsilon\varepsilon}$ are implied conditions.

The covariances on the left hand sides of equations (16b) through (16g) may be estimated from the data, as well as the $\sigma^2_{u_w u_w}$, $\sigma^2_{u_w v_w}$, and $\sigma^2_{v_w v_w}$ terms.

Thus we have seven equations, three constraints, but only three unknowns, α, θ, $\sigma^2_{\varepsilon\varepsilon}$. There are as many as 50 different ways of formulating a solution in this over-determined system, and each should yield reasonably similar estimates of α, θ, and $\sigma^2_{\varepsilon\varepsilon}$, if the model is correct.

We performed this analysis using four different methods for evaluating α, θ, and $\sigma^2_{\varepsilon\varepsilon}$ for the grid cells lying just off New Dungeness. In no case did we find a data set that yielded four estimates of α, θ, and $\sigma^2_{\varepsilon\varepsilon}$ that simply satisfied the constraints, let alone exhibit any consistency. In short, the model, equation (15), did not predict the proper covariance structure.

The reason for this failure may be directly attributed to the errors in the tidal-current model. The variances of the residual velocity components were typically in the range of 10 cm/sec ^{2} to 300 cm/sec ^{2}. The amplitude errors in the tidal-current simulation have been shown to be in the range 10 cm/sec ^{2} to 30 cm/sec ^{2}, which correspond to variances that are equal in size to the residual velocity variances. Thus, $\vec{u}_T - \vec{u}'_T$ is far from negligible, and, in fact, we could argue that most, if not all, of the variability seen in (u_R, v_R) was due to model error and not the wind.

We also performed a number of tests using the Race Rocks wind records, and we tried lagging the wind one hour. None of these tests resulted in a significant relationship.

Figures 16a and 16b show the average residual currents calculated for the days of 25 and 26 August 1978, respectively. These figures show the same intrusion reported in Frisch et al. (1980), and which is also seen in Plates 3d and 3e of Cox et al. (1979). The tidal-current model error is smaller than assuming $\vec{u}'_T$ is zero, and so averages formed using the model should be slightly superior to those made without the model.

SECTION 8

REFERENCES

1. Cannon, G. A. (editor) 1978: Circulation in the Strait of Juan de Fuca: Some Recent Oceanographic Observations, NOAA Technical Report ERL-399-PMEL-29, Environmental Research Laboratories, Boulder, Colorado, 49 pp.

2. Cox, J. M., C. C. Ebbesmeyer, J. M. Helseth 1979: "Surface Drift Sheet Movements Observed in the Inner Strait of Juan de Fuca" Evans-Hamilton Inc. 6306 21st Ave. NE, Seattle, Washington 98115. Completion Report submitted to MESA Puget Sound Project Office, NOAA.

3. Friedman, J. H. and L. C. Rafsky 1979: "Multivariate Generalizations of the Wald-Wolfowitz and Smirnov Two-Sample Tests" The Annals of Statistics Vol. 7, New York, pp. 697-717.

4. Frisch, A. S., J. E. Holbrook, and A. B. Ages 1980: "Observations of a Summertime Reversal in the Circulation in the Strait of Juan de Fuca" submitted to J G R.

5. Godin, G. 1972: The Analysis of Tides, Univ. of Toronto Press, Toronto and Buffalo, 264 pp.

6. Gradshteyn, I. S. and I. M. Ryzhik 1965: Table of Integrals, Series and Products, Academic Press, New York and London, 1086 pp.

7. National Ocean Survey 1973a: Tidal Current Charts, Puget Sound North Part, NOAA, National Ocean Survey, Rockville, Maryland, 12 pp. + endpapers.

8. National Ocean Survey 1973b: Tidal Current Charts, Puget Sound Southern Part, NOAA, National Ocean Survey, Rockville, Maryland, 12 pp + endpapers.

9. National Ocean Survey 1979: Tidal Current Statistics for Puget Sound and Adjacent Waters (unpublished data sets), NOAA, National Ocean Survey, Rockville, Maryland, 38 pp.

10. Overland, J. E., M. H. Hitchman, and Y. J. Han 1979: "A Regional Surface Wind Model for Mountainous Coastal Areas" NOAA Technical Report ERL-407-PMEL-32 Environmental Research Laboratories, Boulder, Colorado, 34 pp.

11. Parker, B. B. 1977: Tidal Hydrodynamics in the Strait of Juan de Fuca - Strait of Georgia, NOAA Technical Report, NOS-69, National Ocean Survey, Rockville, Maryland, 56 pp.

12. Pease, C. H. 1980: An Empirical Model for Tidal Currents in Puget Sound, Strait of Juan de Fuca, and Southern Strait of Georgia, DOC/EPA Interagency Energy/Environment R & D Program Report, in press.

13. Schureman, P. 1958: Manual of Harmonic Analysis and Prediction of Tides, Coast and Geodetic Survey Special Publication No. 98, U.S. Government Printing Office, Washington, D.C., 317 pp.

14. Stewart, R. J. 1978: "Oil Spill Trajectory Predictions for the Strait of Juan de Fuca and San Juan Islands for the Bureau of Land Managements Review of the Northern Tier Pipeline Company's Proposal," Pacific Marine Environmental Laboratory, NOAA Environmental Research Laboratories, Seattle, Washington.

APPENDIX A

CALCULATION OF TIDAL PHASE AND AMPLITUDE FROM MODEL COEFFICIENTS

The tidal model is based on the 5 constituents found in Table 4 of Parker (1977), M_2, S_2, N_2, K_1, and O_1. Parker's Epochs (or phase lag) are measured with respect to local time (LT). Since the model also uses LT at the subprogram level, the phase for one of the constituents is given by:

$$\theta^p_{t\ell} = (V_o + u) - (\kappa)^p_{t\ell} \tag{A1}$$

where p denotes Parker's station number, ℓ denotes the tidal constituent (e.g., M_2,N_2, etc.), t denotes local time, and the "equilibrium argument," (V_o + u), is taken from Table 15 of Schureman (1958). The time in the model is measured relative to 0000 January 1, 1978, and, for example, the equilibrium argument for the M_2 constituent is 201.8°.

The major axis velocity of one of the model's reference stations thus assumes the following form:

$$V^p_\ell(\tau) = A^p_\ell \cos\ (\sigma_\ell \tau + \theta^p_{t\ell}) \tag{A2}$$

where the superscript again denotes the reference station number, and the subscript denotes the tidal constituent. Note that the model calculation is based on arrays of $\theta^p_{t,\ell}$ and not on the epoch, κ, and equilibrium argument.

The simulated current for tidal constituent "ℓ" at a grid location (i,j) is determined from the summation of as many as three, weighted, reference station velocities. Thus:

$$\begin{aligned} V_\ell{}^{i,j}(t) &\equiv a^{i,j}_\ell \cos\ (\sigma_\ell t + \sigma^{i,j}_{t,\ell}) \\ &= \sum_{m=1}^{3} W(i,j,m) A^{p(i,j,m)}_\ell \cos(\sigma_\ell \tau + \theta^{p(i,j,m)}_{\tau,\ell}), \end{aligned} \tag{A3}$$

where the reference station index, P(i,j,m), and weighting factor W(i,j,m) are determined from arrays in which the east-west and north-south positions determine the principal indices i and j. The index 'm' is just the summation index and is of no further consequence. Our present discussion is devoted to the demonstration that equation (A3) is properly implemented in the model.

Dispensing with the cumbersome notation of (A3) we can see that our simulated tidal current for constituent, K, is created numerically using an equation of the general form:

$$A_k \cos(\sigma\tau + \phi_k) = \sum_{m=1}^{3} b_m^k \cos(\sigma\tau + \theta_m^k)$$

The problem is to evaluate a_k and ϕ_k in terms of the b_m^k and θ_m^k parameters. This is readily done by expanding the cosine function with its $(\sigma t + \theta_m^k)$ argument into sine and cosine constituents of argument σt, each multiplied by sines and cosines of argument θ_m^k, (or θ_m^σ) and the b_m^k (or a_k) amplitudes. This results in two equations for ϕ_k and a_k:

$$\phi_k = \tan^{-1}\left\{\frac{\sum_{m=1}^{3} b_m^k \sin\theta_m^k}{\sum_{m=1}^{3} b_m^k \cos\theta_m^k}\right\} \qquad \text{(A4a)}$$

$$a_k = \left\{\left(\sum_{m=1}^{3} b_m^k \sin\theta_m^k\right)^2 + \left(\sum_{m=1}^{3} b_m^k \cos\theta_m^k\right)^2\right\}^{\frac{1}{2}} \qquad \text{(A4b)}$$

These are the phase and amplitude of the simulated tidal current assuming the model is functioning properly. They are to be compared with the R2SPEC analysis of a time series generated by the model.

The model creates its simulated time series through the summation of the five tidal constituents mentioned above. Thus,

$$V^{i,j}(t) = \sum_{\ell=1}^{5} V_\ell^{i,j}(t) \qquad \text{(A5)}$$

This velocity lies along an axis determined by the flood-ebb direction. It is converted to u (east-west), v (north-south) components with a simple rotation transformation. It is this time series of u, v components that comprise the data analyzed by R2SPEC.

The only difficulty in this comparison is the conversion of the model phase lag parameters into forms suitable for comparison with R2SPEC's output. R2SPEC lists the constituent Epochs in a form consistent with Schureman (1958), which is to say that it is referenced to GMT time, not local time. The conversion is made as follows:

$$(\kappa)_{t,\ell}^{i,j} = (V_0 + u)_\ell - \theta_{t,\ell}^{i,j} \text{ (see Eq. (A1))},$$

and

$$(\kappa)_{T,\ell}^{i,j} = (\kappa)_{t,\ell}^{i,j} + \sigma_\ell * (8 \text{ hrs.}) \qquad \text{(A6)}$$

where T denotes GMT time and σ_ℓ is constituent ℓ's frequency in degrees per hour.

APPENDIX B

MOMENTS FOR RANDOMLY ORIENTED CONSTITUENT DISPLACEMENTS

If the major axis of the ℓth constituent is randomly oriented with respect to a reference axis, then the amplitude of the motion along the reference axis will be given by the product

$$x = \delta\cos\phi_\ell \cos\xi_\ell; \tag{B1}$$

where δ is the amplitude of the motion,

ϕ_ℓ is the angle between the reference axis and the axis of motion, and

ξ_ℓ is the phase of motion.

We assume ϕ_ℓ and ξ_ℓ are independent, uniformly distributed random variates lying in the interval $(0,2\pi)$.

We now define $y = \delta\cos\phi_\ell$ and $z = \cos\xi_\ell$, and note that the distributions on y and z are given by:

$$f_z(z) = \frac{1}{\pi(1-z^2)^{\frac{1}{2}}}; \quad f_y(y) = \frac{1}{\pi\delta(1-\left(\frac{y}{\delta}\right)^2)^{\frac{1}{2}}}; \tag{B2a,b}$$

where $-1 \leq z \leq +1$, and $-\delta \leq y \leq +\delta$.

For x_0 greater than zero, we can readily derive the probability that x is less than or equal to x_0:

$$P[x \leq x_0] = 1-2\int_{x_0}^{\delta} dy \int_{\frac{x_0}{y}}^{1} dz\, f_{y,z}(y,z) = 1-2\int_{x_0}^{\delta} dy\, f_y(y)[1-F_z(\tfrac{x_0}{y})]; \delta > x > 0 \tag{B3}$$

where F_z is the cumulative distribution on z.

The marginal distribution is obtained by taking the derivative of the cumulative distribution, $P[x \leq x_0]$, whence:

$$f_x(x_0) = \int_{x_0}^{\delta} \frac{2dy}{\pi^2(\delta^2-y^2)^{\frac{1}{2}}(y^2-x_0^2)\pi}; \quad \delta \geq x_0 \geq 0. \tag{B4}$$

Using similar arguments, a corresponding form can be found for $-\delta \leq x_0' \leq 0$. Upon inspection, it will be seen that the equation for $-\delta \leq x_0' \leq 0$ is just a transformation of (B4) in which $x_0' = -x_0$. Thus, (B4) holds for the whole range of x, $-\delta \leq x_0 \leq \delta$.

The integral (B.4) can be integrated in terms of elliptic integrals of the first kind, with the result:

$$f_x(x_0) = \frac{2}{\pi^2}\,\frac{1}{\delta}\,F\left(\frac{\pi}{2},\ 1-\left(\frac{x_0}{\delta}\right)^2\right) \qquad (B5)$$

(See Gradshteyn and Ryzhik, 1965, §3.152(10) pg 246.)

This form can then be used to find the higher moments of the distribution. The function is symmetrical with $-\delta \leq x \leq \delta$, and so all odd moments are zero. The second moment is found as follows:

$$E(x^2) = \left(\frac{2}{\pi}\right)^2 \int_0^{\delta} \frac{1}{\delta}\,K\left(1-\left(\frac{x}{\delta}\right)^2\right) x^2 dx$$

$$= \left(\frac{2}{\pi}\right)^2 \delta^2 \int_0^1 \frac{E(k)}{2} dk \,. \qquad \text{(G. and R., §6.147, pg 637)}$$

$$= \left(\frac{2}{\pi}\right)^2 \delta^2\,\frac{1}{2}\left\{\frac{1}{2} + G\right\} = .2865\,\delta^2. \qquad \text{(G. and R., §6.148, pg 637)}$$

where $K(k) = F\left(\frac{\pi}{2},k\right)$, is the complete elliptic integral; and

$G = .915\ 965\ 594\ldots,$

is Catalan's constant. Higher moments can be readily deduced from §6.147.

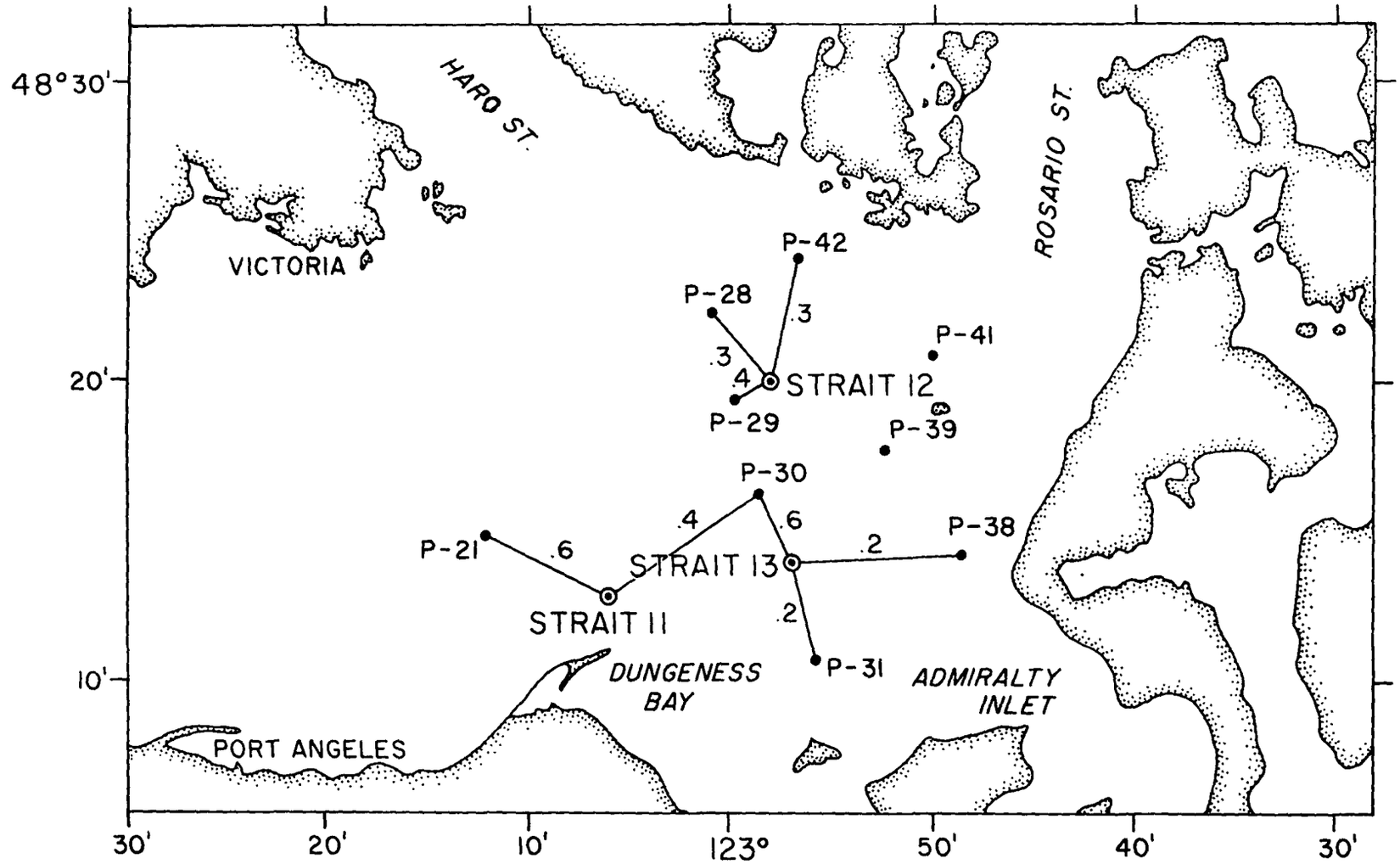

Figure 1. Location of Straits 11, 12, and 13, and the weighting factors applied to Parker's stations.

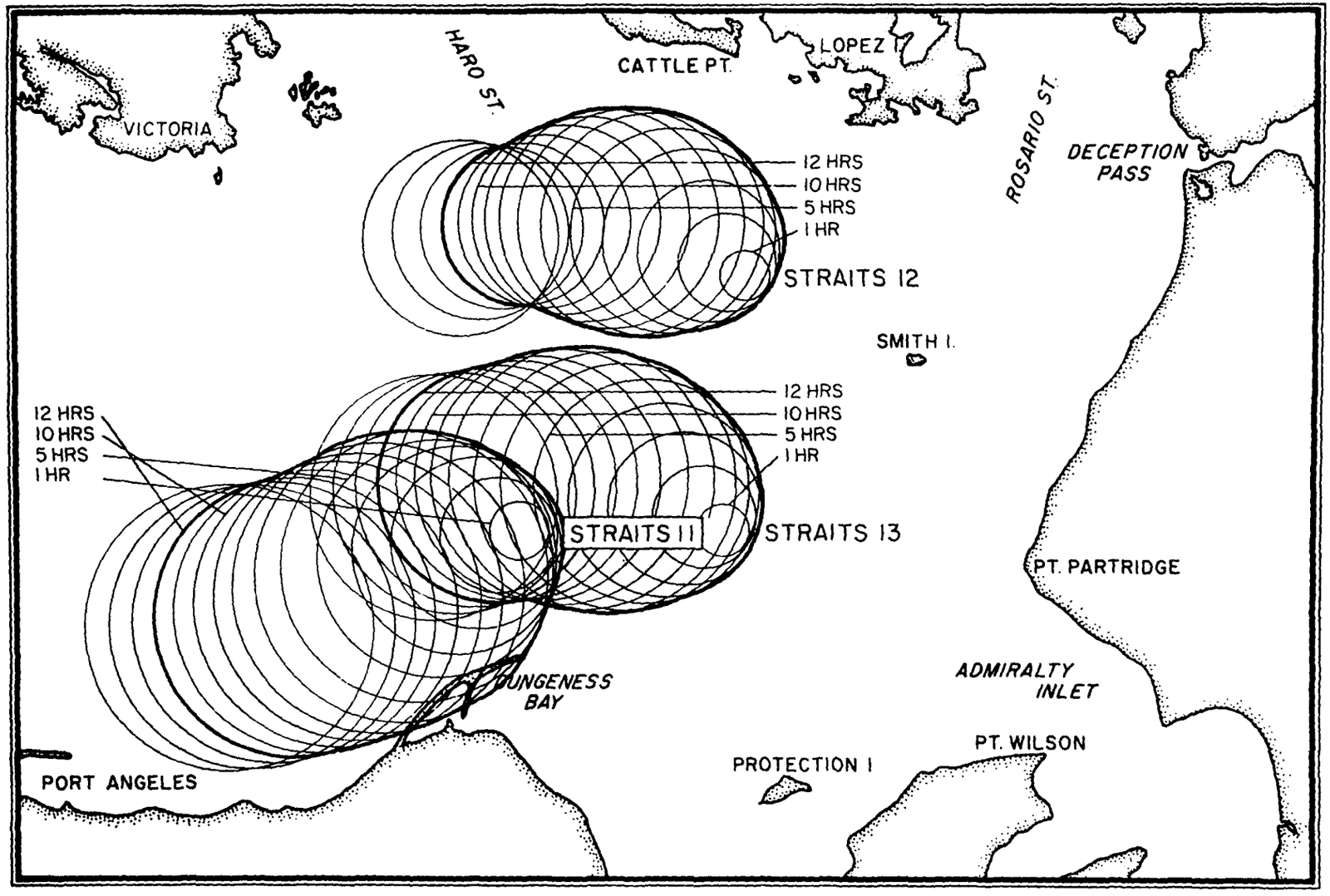

Figure 2. Dispersion envelopes assuming no knowledge of tidal currents (Case 1).

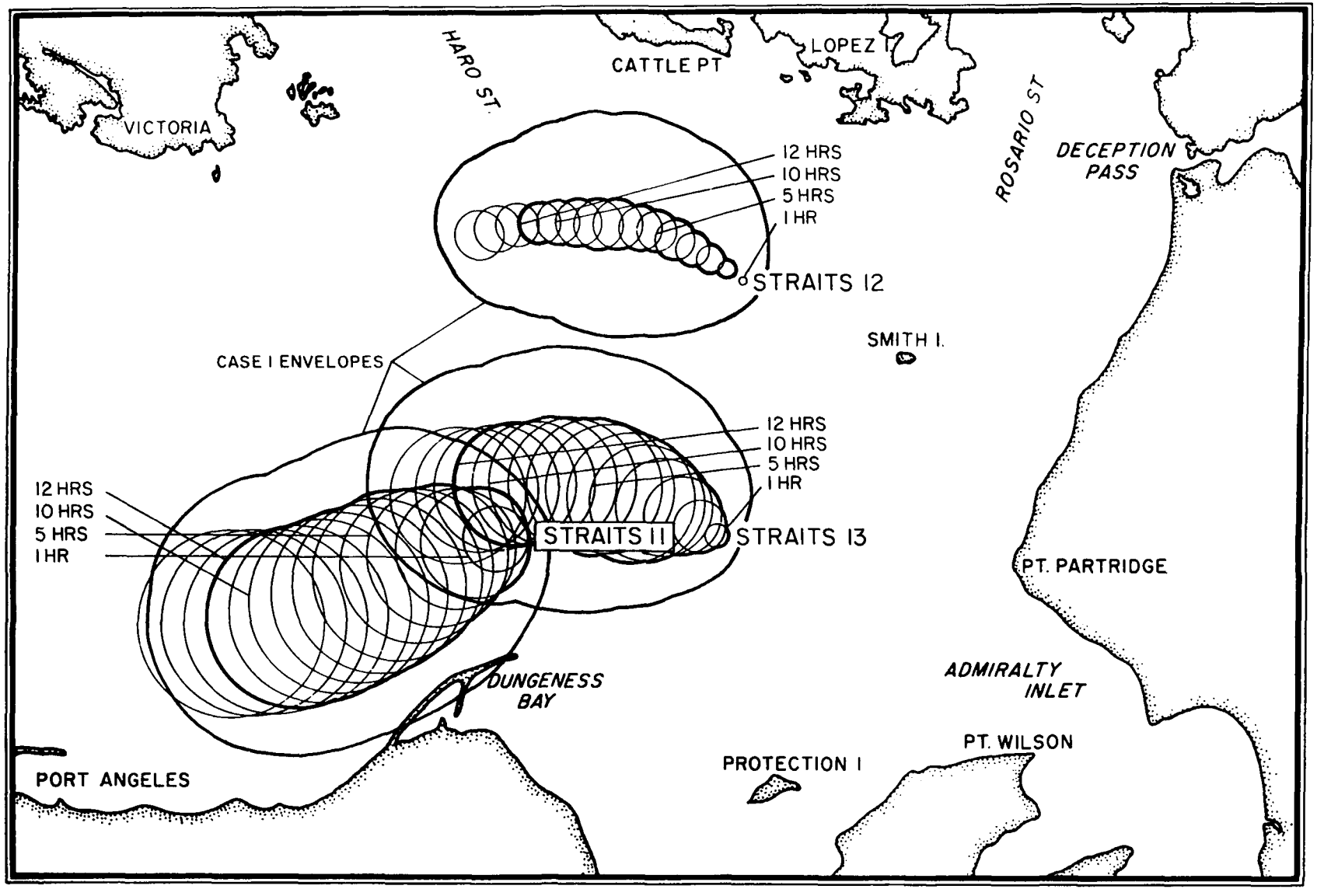

Figure 3. Tide model contribution to reducing position error relative to Case 1.

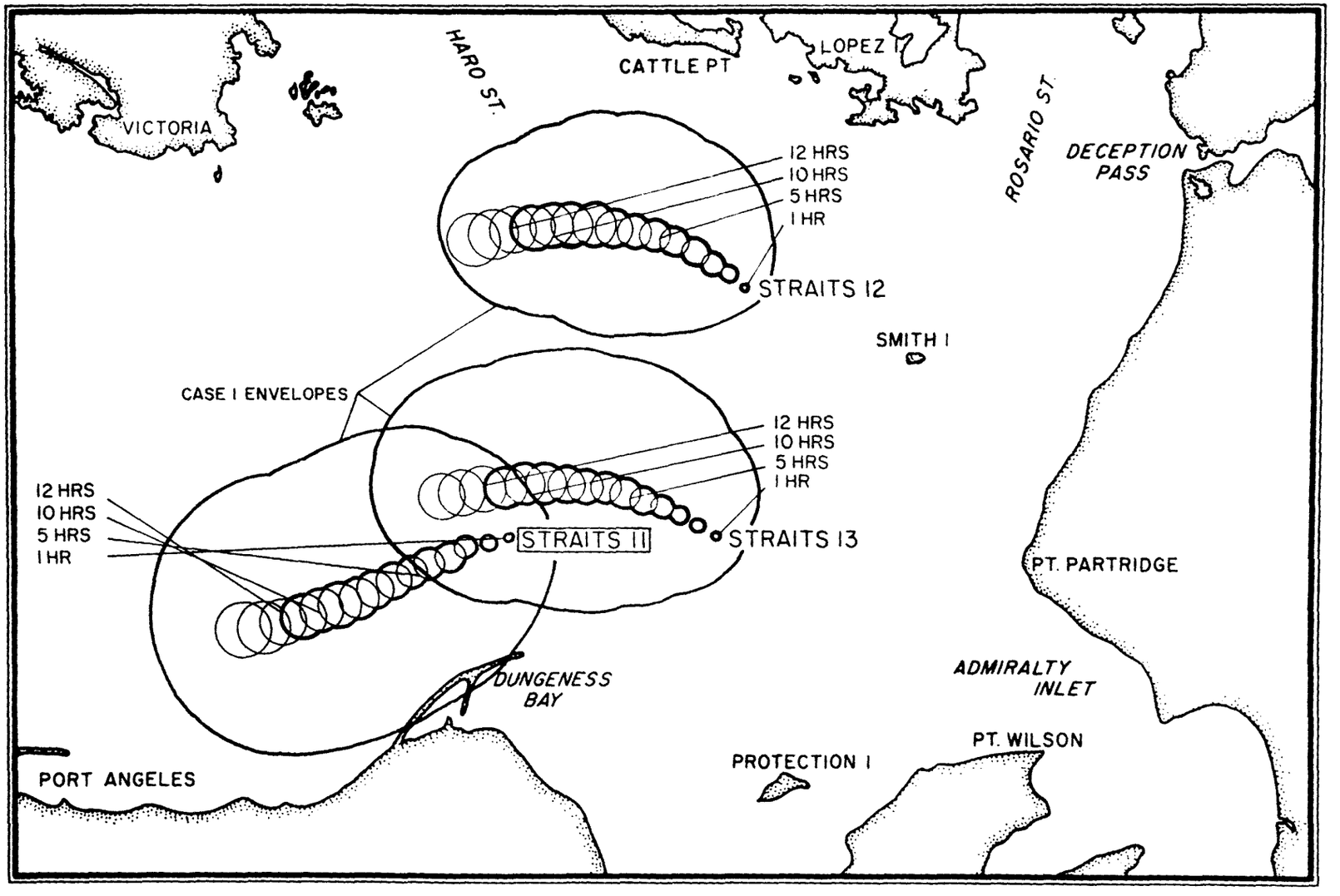

Figure 4. Dispersion envelopes associated with ignorance of high frequency non-tidal current oscillations (Case 2).

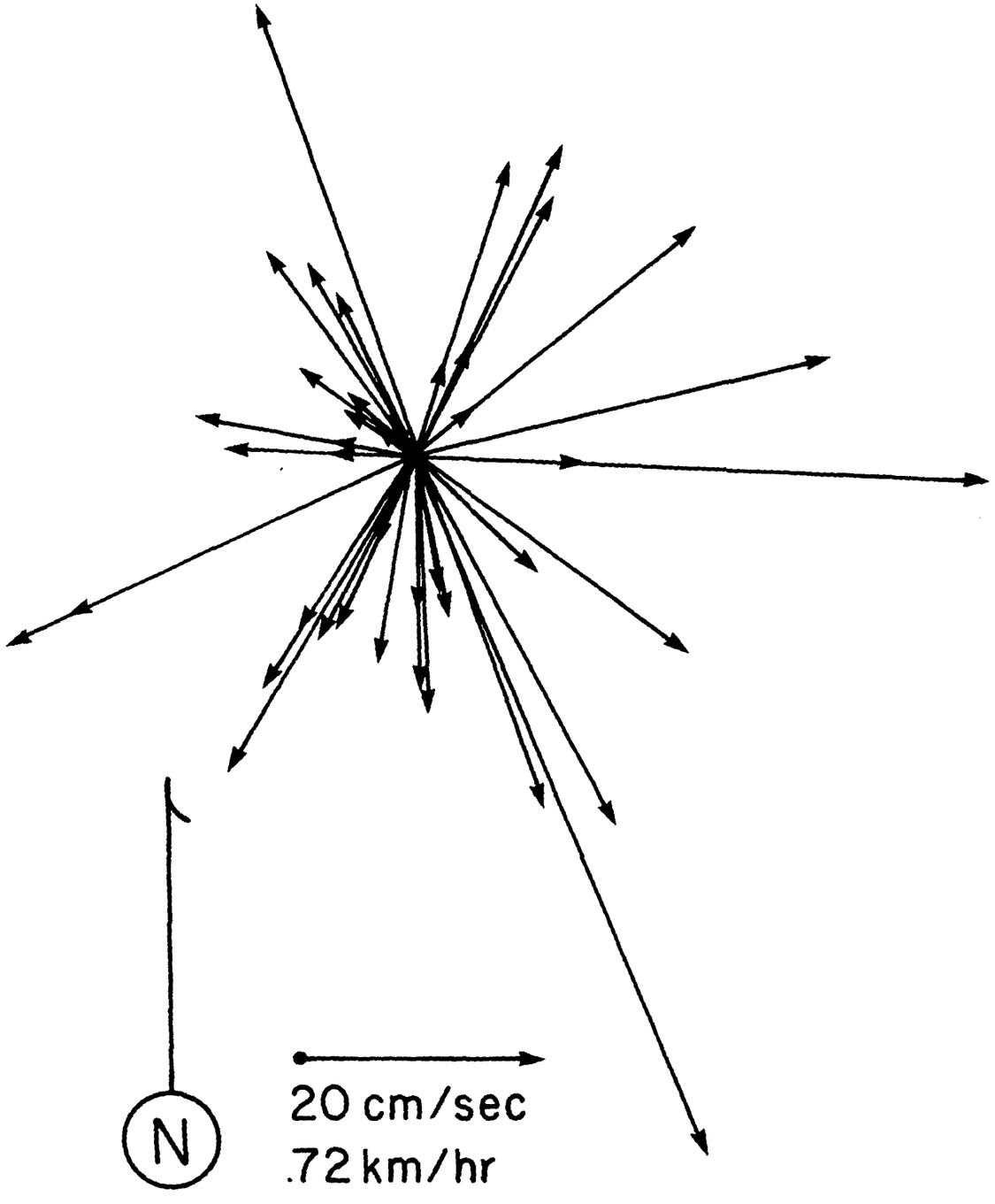

Figure 5. Observed net currents at various locations in the Strait of Juan de Fuca and the Central Basin.

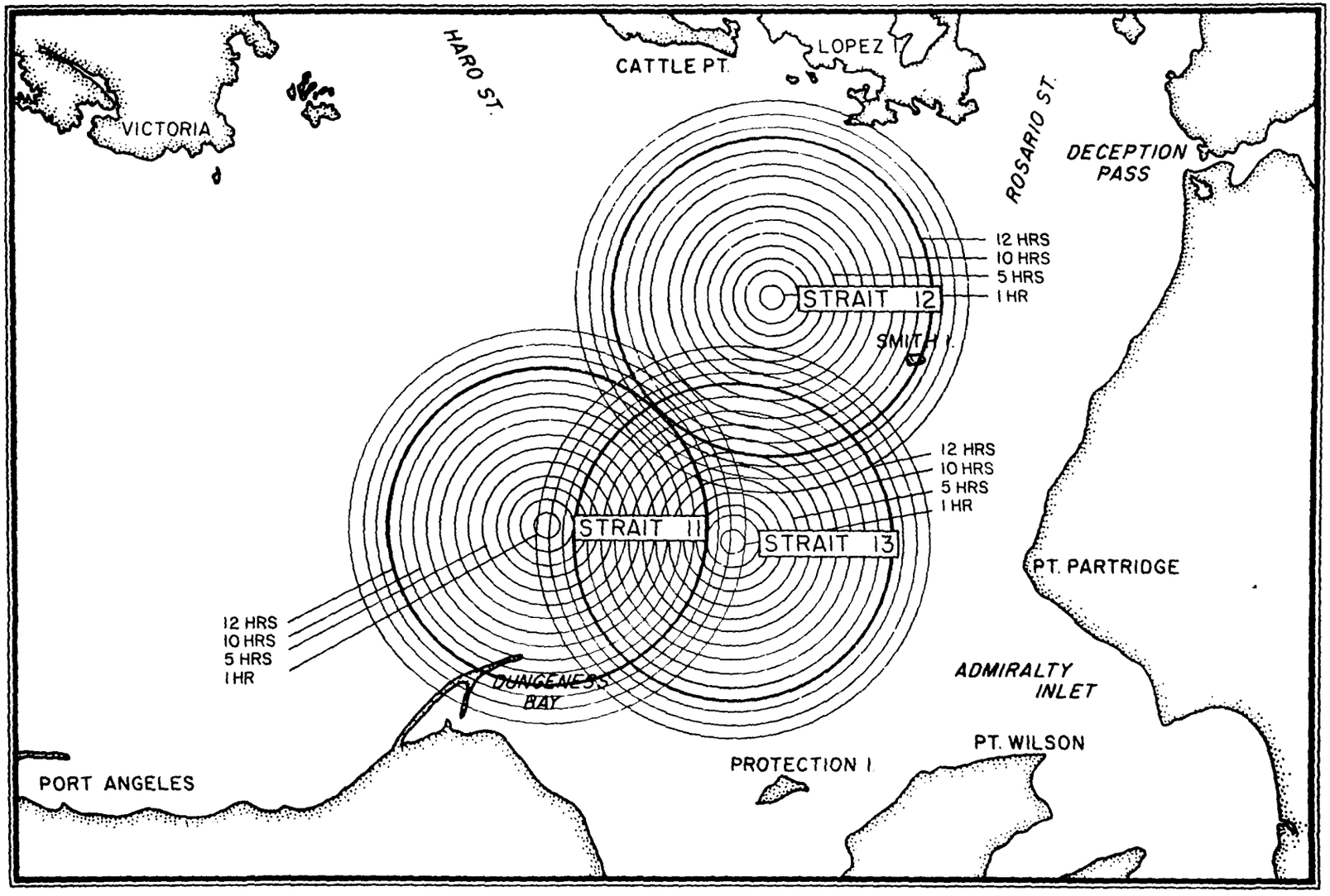

Figure 6. Dispersion caused by randomly oriented net current of .66 km/hr (case 2).

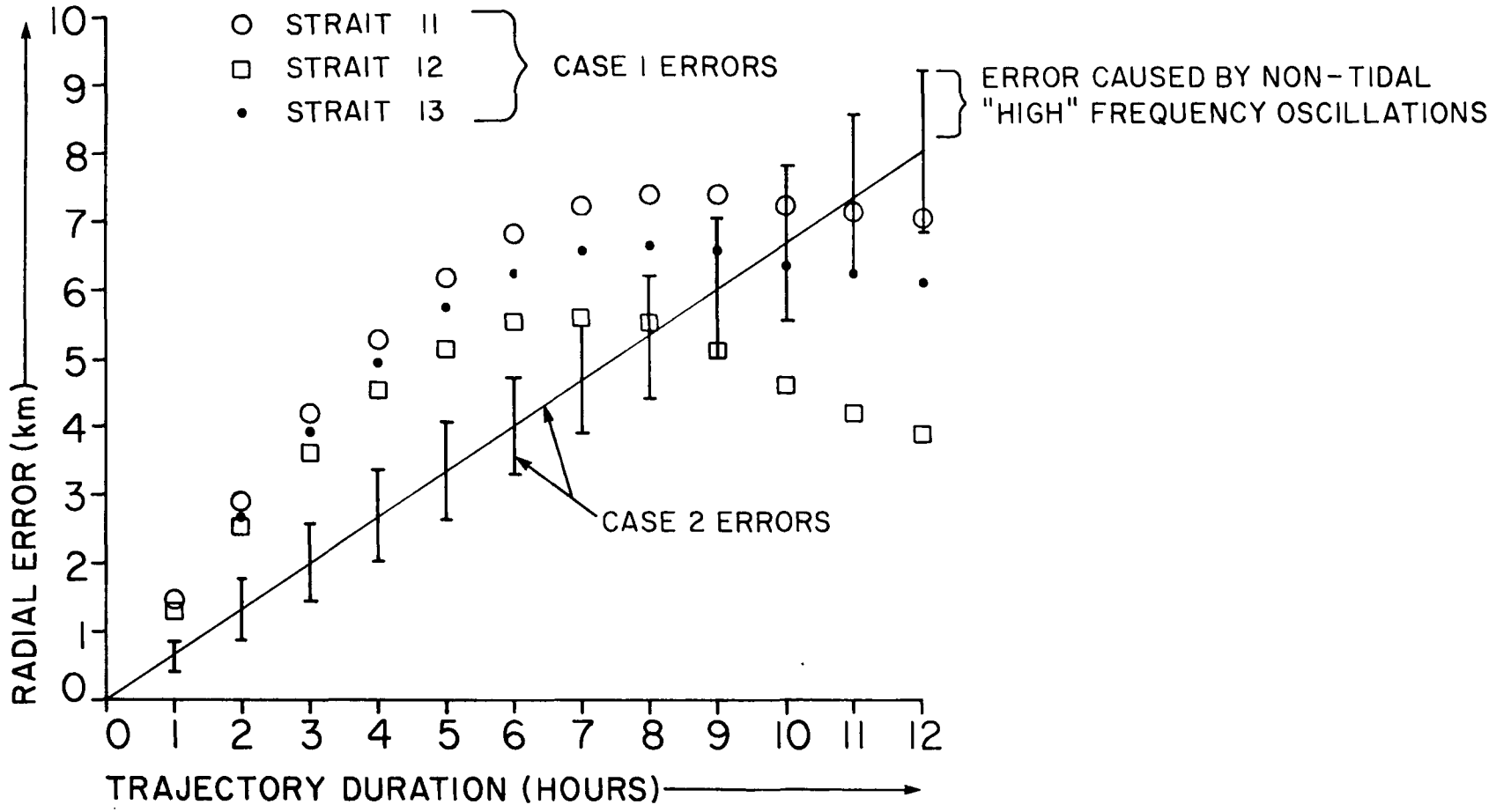

Figure 7. A comparison of Case 1 and Case 2 errors.

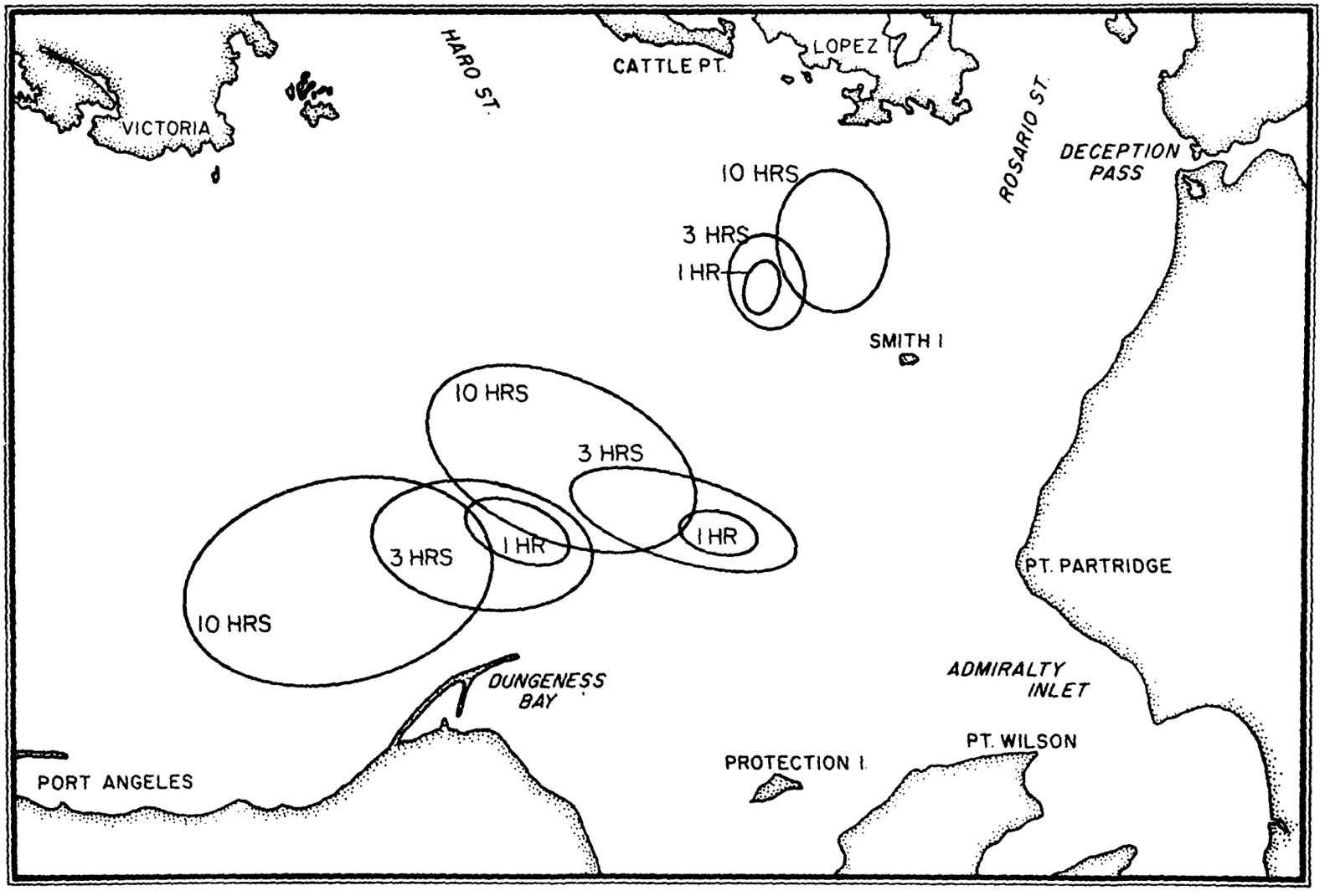

Figure 8. Difference - current dispersion ellipses at 1, 3, and 10 hours.

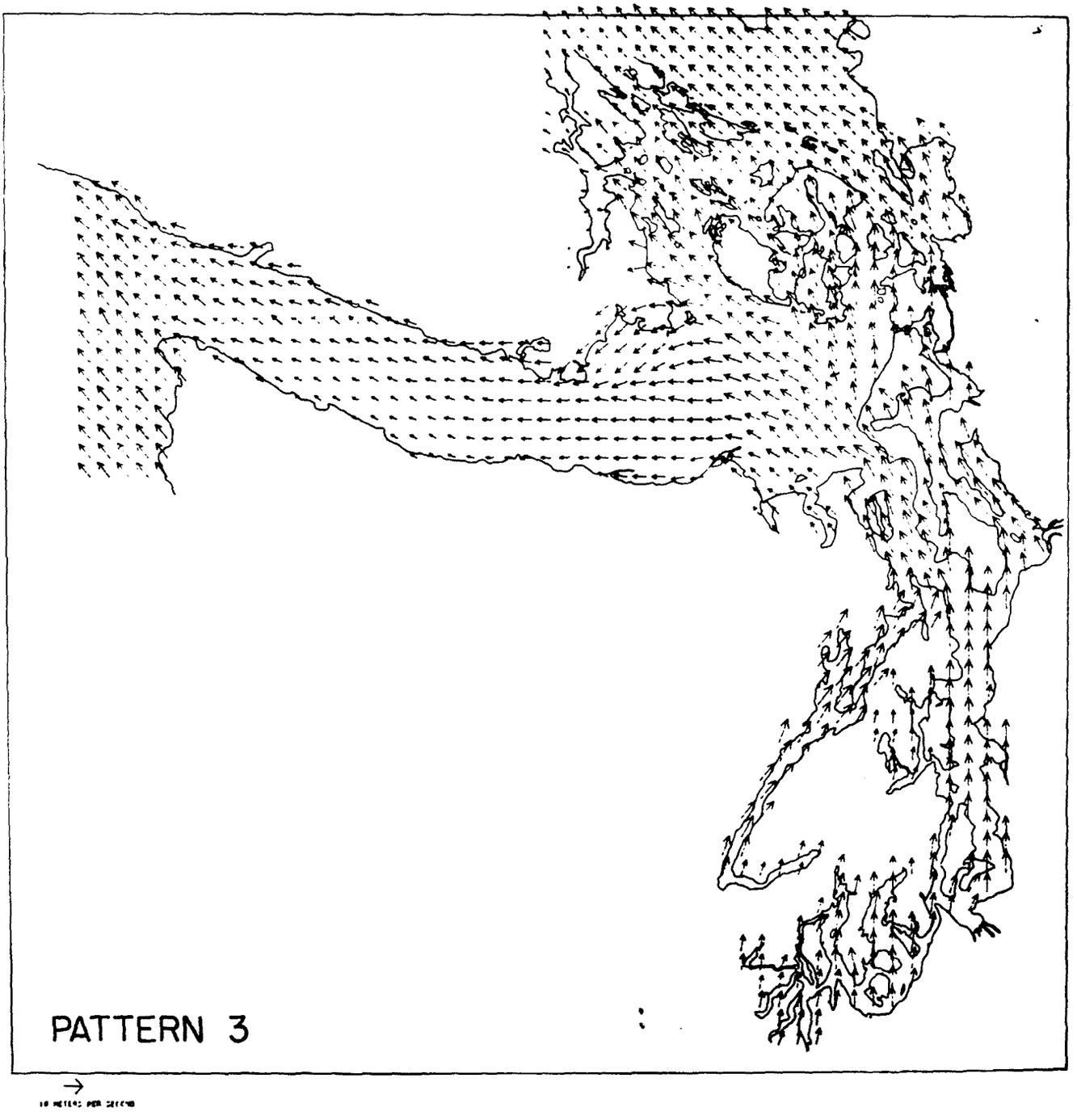

Figure 9. Wind Pattern No. 3

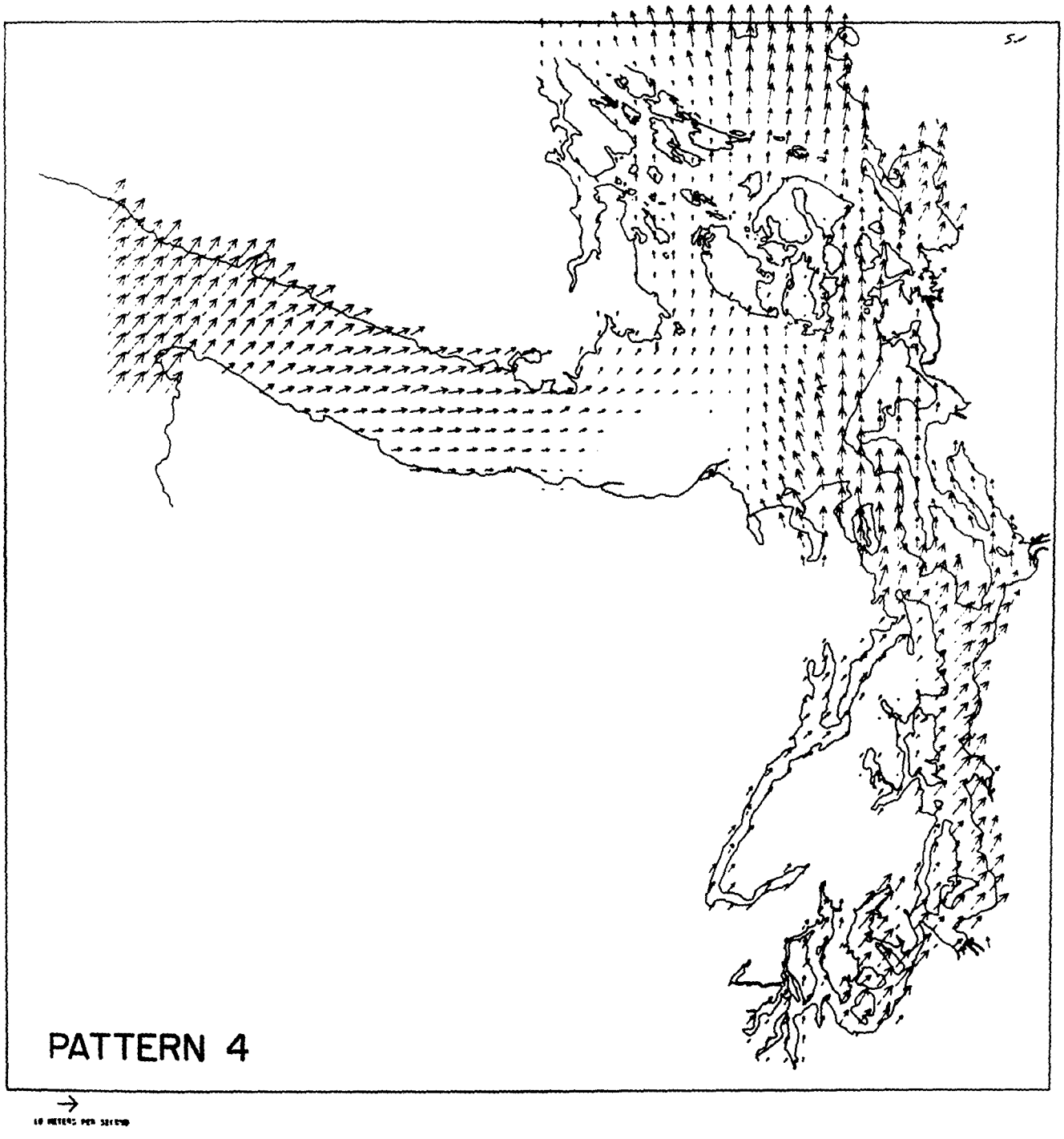

Figure 10. Wind Pattern No. 4

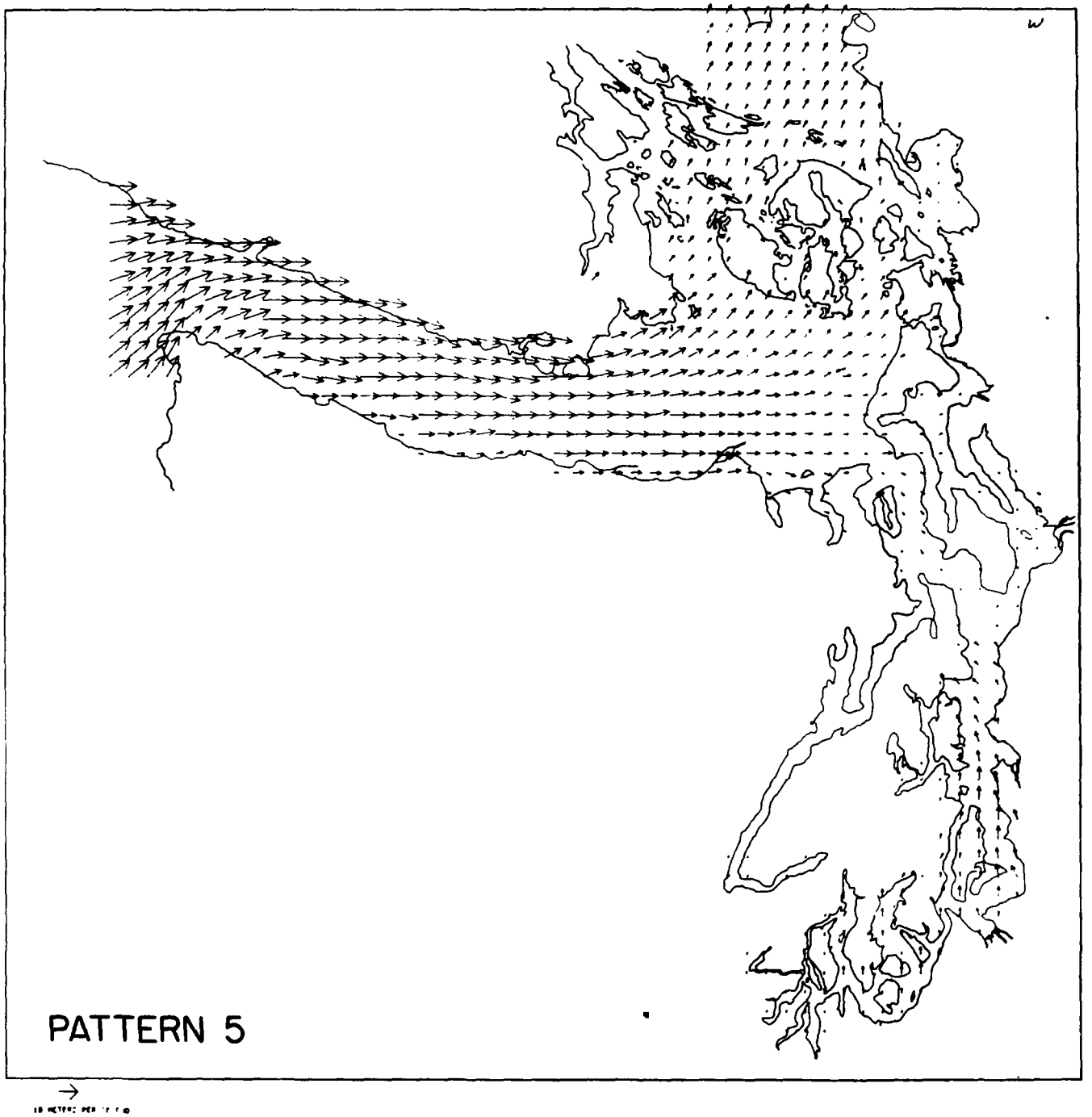

Figure 11. Wind Pattern No. 5

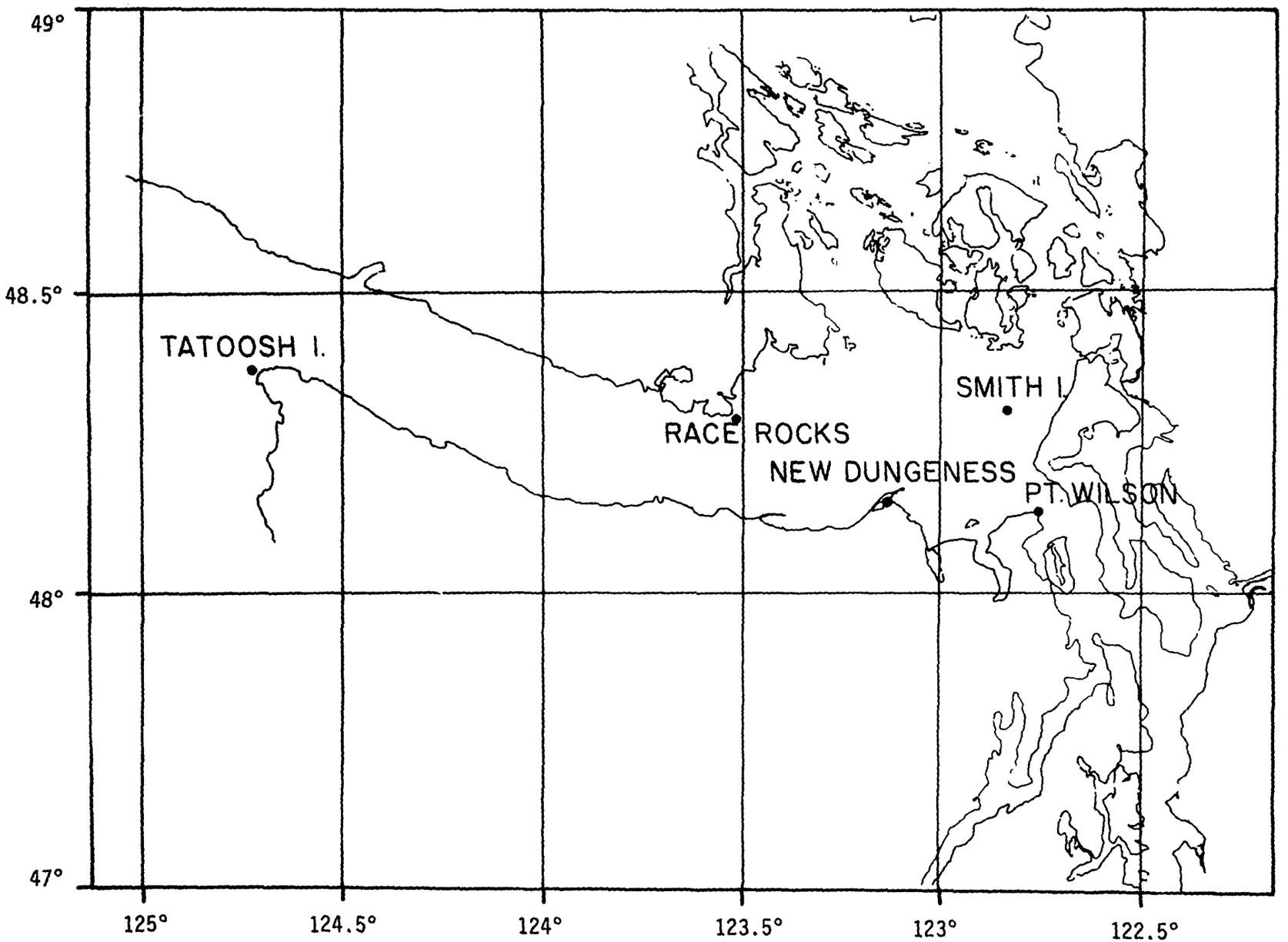

Figure 12. Wind station locations.

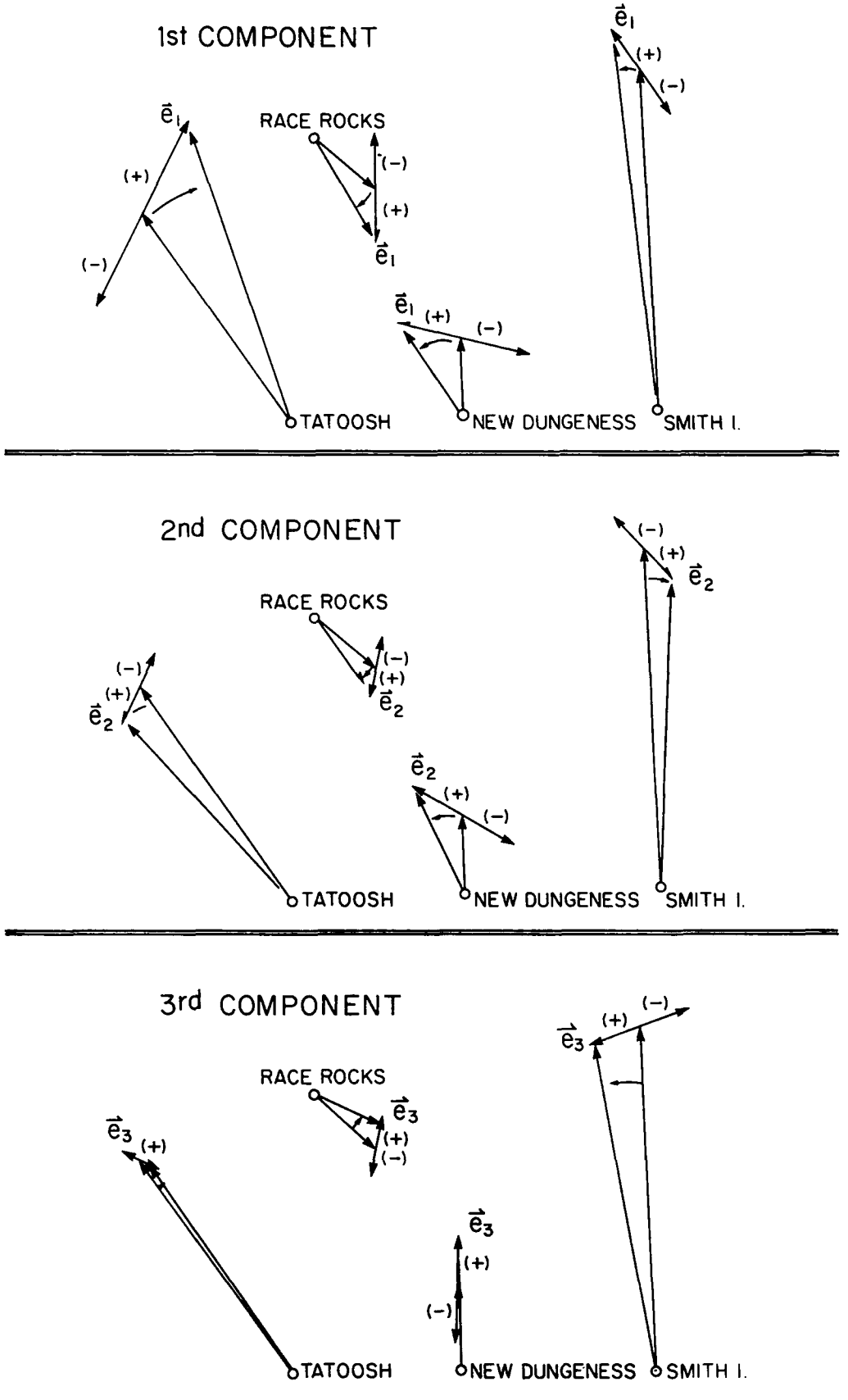

Figure 13. Principal components of surface wind observations.

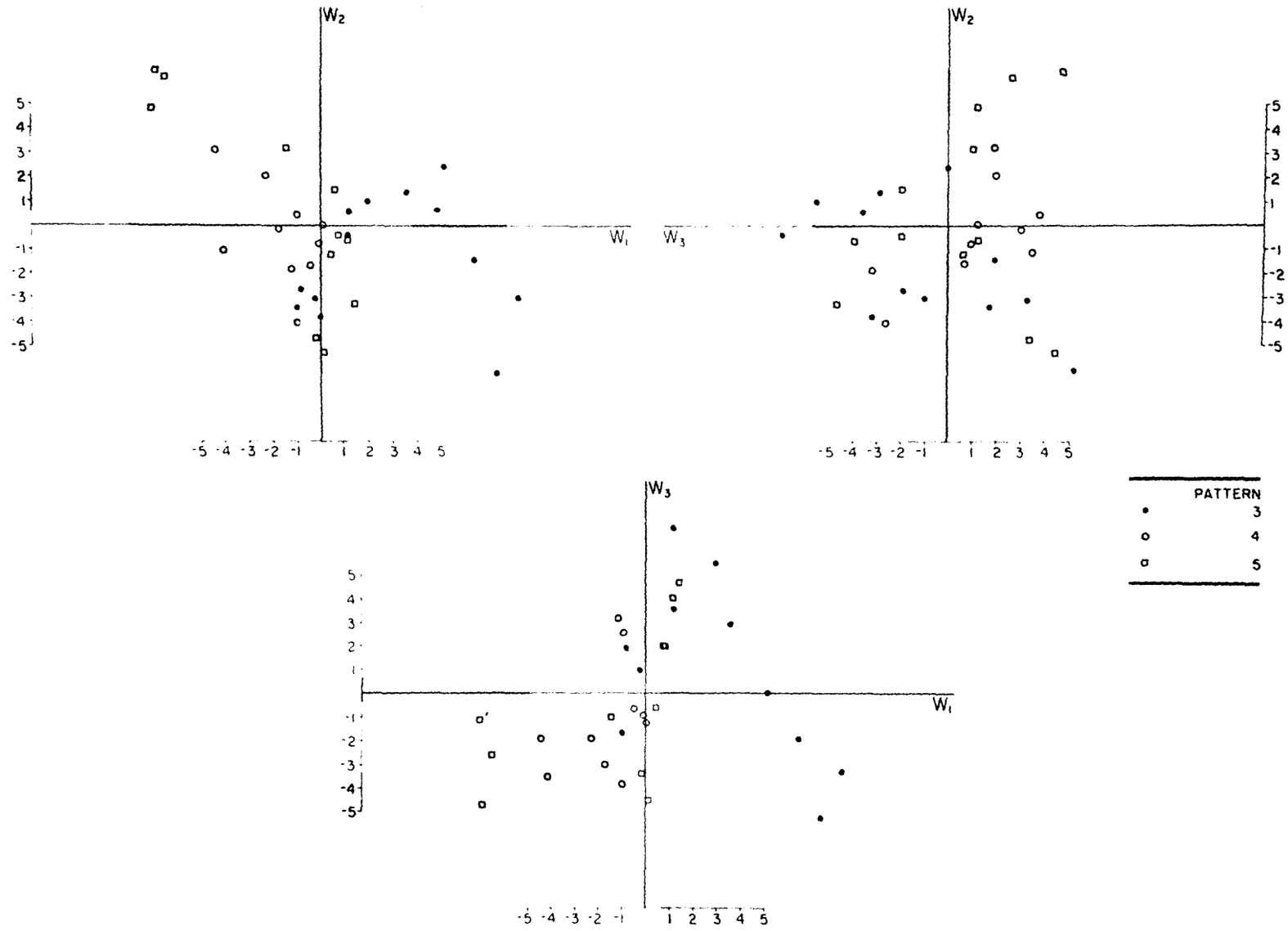

Figure 14. Scatter plot of principal component weights.

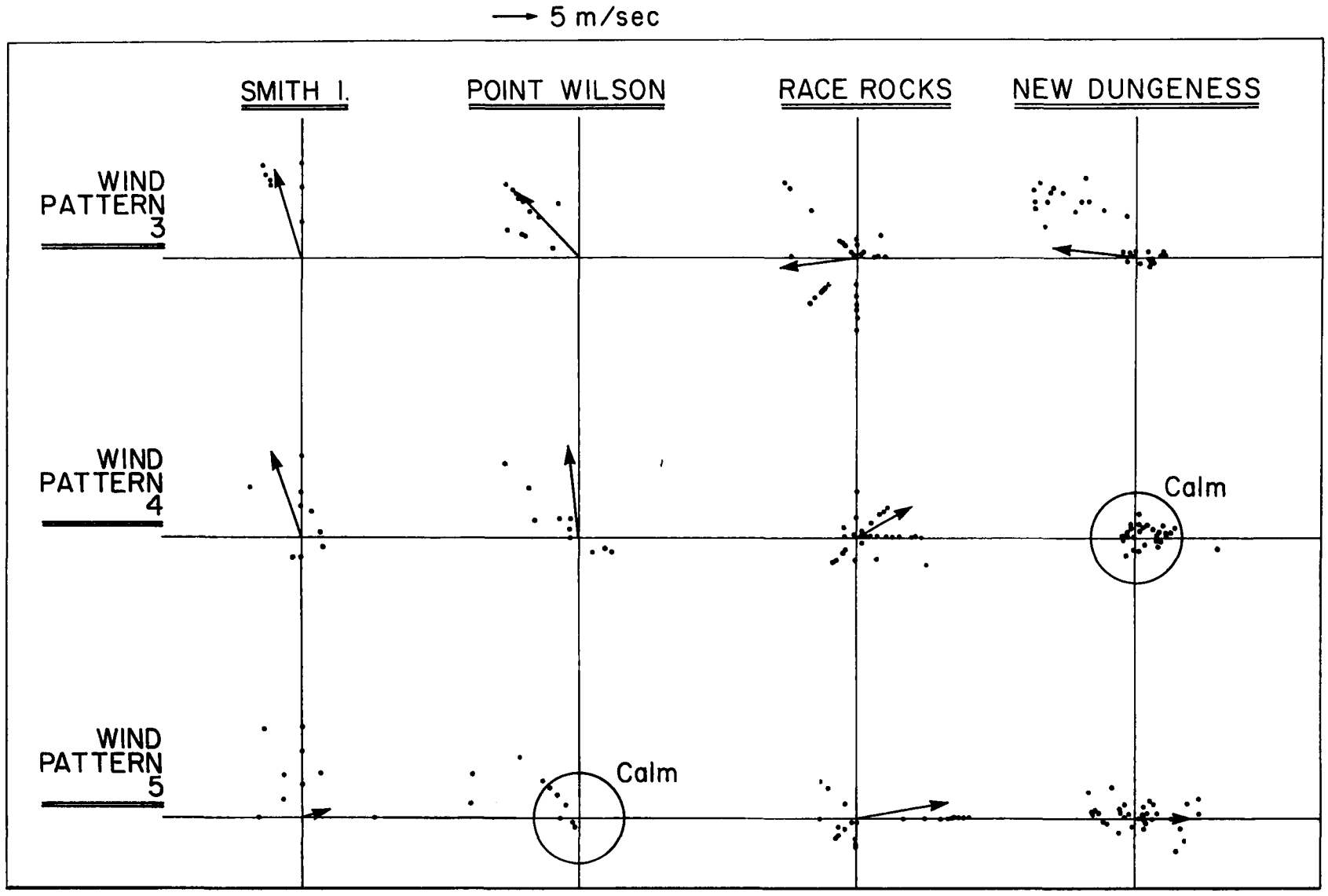

Figure 15. Scatter plot of wind observation, sorted by pattern type at four central basin stations.

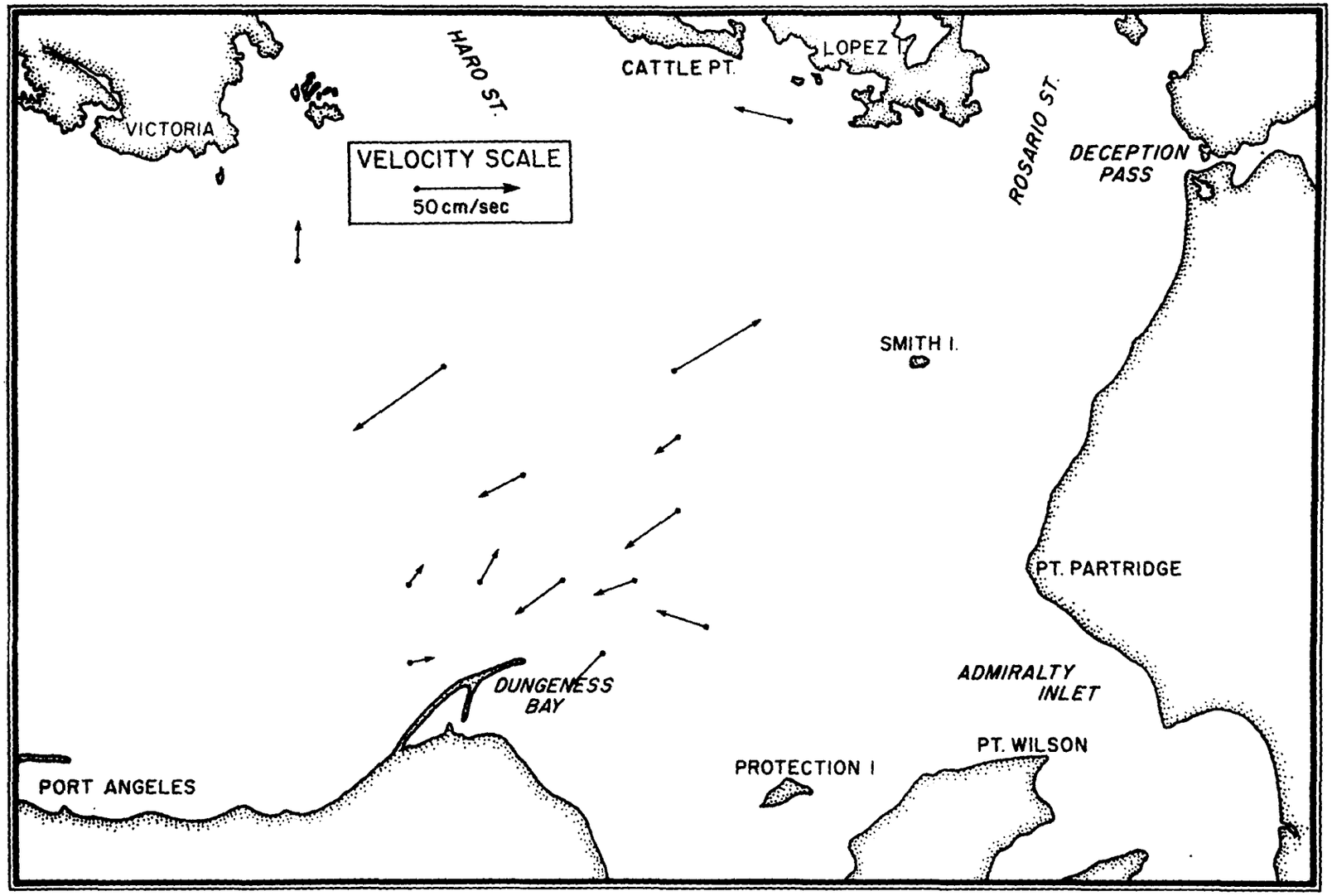

Figure 16a. Average residual currents on August 25, 1978 (residual = drifter - model).

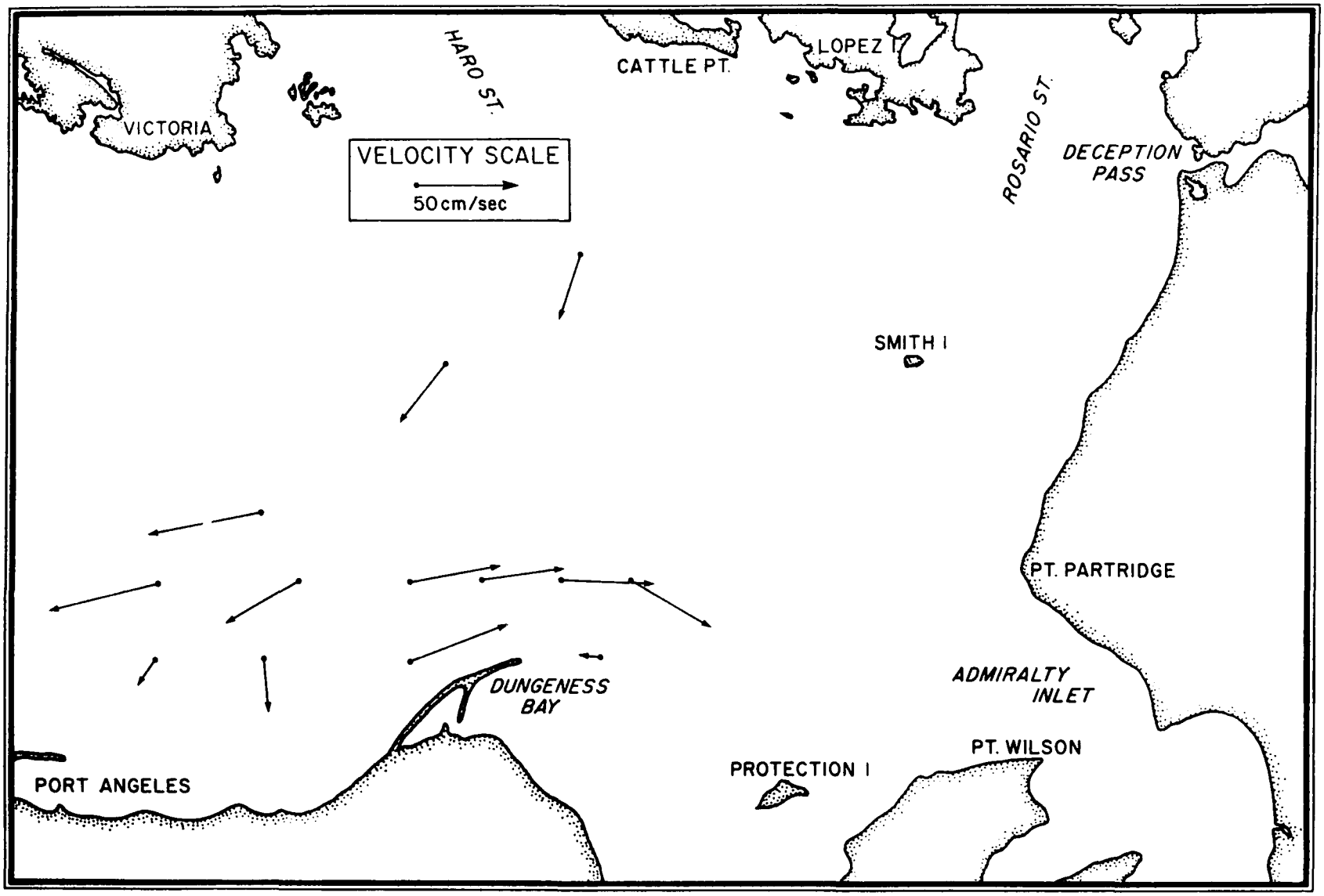

Figure 16b. Average residual currents on August 26, 1978 (residual = drifter - model).

NOAA/OTS CHEMICAL LIBRARY
401 M ST., S.W., TS-793
WASHINGTON, D.C. 20460

* GPO 797-412 1981